Membrane Interactions at the Molecular Level Using the Surface Force Apparatus

By

RAQUEL OROZCO-ALCARAZ
B.S. Chemical Engineering (University of California, Berkeley) 2006

DISSERTATION

Submitted in partial satisfaction of the requirements for the degree of
DOCTOR OF PHILOSOPHY
in
Chemical Engineering
in the
OFFICE OF GRADUATE STUDIES
of the
UNIVERSITY OF CALIFORNIA
DAVIS

Approved:

_____
Tonya Kuhl, Chair

_____
Marjorie Longo

_____
Roland Faller

Committee in Charge

2012

ProQuest LLC.
789 East Eisenhower Parkway
P.O. Box 1346
Ann Arbor, MI 48106 - 1346

Table of Contents

Overview

Raquel Orozco-Alcaraz
December 2012
Chemical Engineering

Membrane Interactions at the Molecular Level Using the Surface Force Apparatus

Abstract

Measurements of biological membranes can have significant impact in the area of biosensor design, drug delivery, and understanding of living cells. The Surface Force Apparatus (SFA) has been used extensively to measure the interaction forces between surfaces of model lipid-membranes. In this work, the SFA was used to measure the interaction forces between three different biological membrane systems not previously studied. The systems considered in this work are: 1) silica-supported membranes formed by Langmuir-Blodgett deposition of 1,2-dipalmitoyl-*sn*-glycero-3-phosphocholine (DPPC); 2) mica-supported fluid membranes containing polyethylene glycol (PEG) functionalized lipids; 3) interaction between molecularly smooth mica and live endothelial cell surfaces. A systematic study of analytical models was first completed to institute a way to properly process the raw data from the complex interferometry systems used in this work. The types of forces involved in the measurements are predominantly characterized by short range steric repulsion, long-range electrostatic interactions, and mid-range attractive Van der Waals. For the studies on silica-immobilized DPPC

membranes, findings suggest that the physisorption of lipid membrane to mica is stronger than that for glass, resulting in a long range electrostatic repulsion due to the imperfect screening of the charged substrate. In the experiments performed using PEGylated fluid lipid-membranes, it was established that the lateral diffusivity of the bilayer is affected under confined geometries. For the endothelial cell measurements, it was shown that the SFA provides the sensitivity to extract elastic properties of live cells surfaces under small deformations. The measurements performed and their results give an insight of the newfound capabilities of the Surface Force Apparatus.

CHAPTER 1

Experimental comparison between multilayer matrix model (MMM) and the 3-layer and 5-layer multiple beam interferometry (MBI) models

Modified with permission from Raquel Orozco-Alcaraz and Tonya L. Kuhl. Impact of membrane fluidity on steric stabilization by lipopolymers (Supplemental Information). *Langmuir*, **2012**.

Abstract

In this work, experimental data is used for the first time to compare and report the distance between interfacial surfaces using different methods of analysis: The multilayer matrix model (MMM), and two analytical solutions based on multiple beam interferometry (MBI). A detailed description for the inputs of the MMM algorithm is included and, for completeness, the analytical solutions for a 3 and 5-layer interferometer are shown. We find that the 3-layer analytical method, the most popular and widely used in SFA analysis, provides only a good first approximation to the 5^{+}-layer interferometer. For a 5-layer interferometer it is more desirable to use the MMM or the 5-layer analytical method at smaller distances. We also show that for large interfacial distances, however, the difference between these methods is minimal and thus any of the three methods is functional.

Introduction

The surface force apparatus has been used extensively over the years to measure the interacting forces between two surfaces[1-5]. The primary objective in surface force apparatus (SFA) interferometry measurements is to determine the distance (or separation) between the substrates. The distance is determined from the wavelength positions of the fringes of equal chromatic order (FECO) formed from the constructive interference of light passing through the surfaces. The interferometry data from the surface force apparatus (SFA) is analyzed by solving the optical equations using a multilayer matrix model (MMM) or analytical solutions based on multiple beam interferometry (MBI).

MMM, described previously[6-9], is derived from Maxwell's equations and can be used to numerically calculate the FECO wavelengths obtained from an optical interferometer if the thickness and refractive index (RI) of each layer in the interferometer are known[7, 9]. Analytical expressions based on MBI exist for 3 and 5-layer symmetrical interferometers.[2] Note that in MBI, the silver layers are not accounted for in the calculations whereas in MMM all layers are taken into consideration. Thus every time we describe the number of layers in MMM, the silver layers are included. This means that for the same interferometer in MMM notation has two extra layers than MBI notation. For asymmetric systems or when more than 7 layers are involved MMM is employed.

Our measurements are based on the interaction between lipid bilayers deposited on SiO_2-coated mica back silvered surfaces in water. This system requires a MMM solution of a 9-layer interferometer. In this supplement we describe our in-house MMM algorithm and the steps we take to establish the thickness and refractive index for each layer in the interferometer. Finally, we demonstrate that the analytical 5-layer MBI solution is a very good approximation to the more complicated MMM approach for obtaining surface separation or gap thickness.

Materials and Methods

Chemicals, Sample Preparation, Surface Force Measurements.

Refer to Chapter 2 for details.

MMM algorithm used for analysis:

We have developed both Mathematica and MatLab MMM algorithms to fit the thickness and refractive index from each layer in the optical interferometer. The algorithm closely follows what was proposed by Clarkson[7] and Mangipudi[9]. The program essentially matches the wavelength peaks of FECO measurements with the appropriate layer thickness and refractive index for each layer. The following are the program inputs and approach:

1. Wavelength peaks of FECO obtained from a spectrometer coupled to the SFA.
2. Wavelength peaks from the Hg spectrum (green and yellow lines), which are used as a calibration tool.
3. Estimated or known thickness (minimum, maximum) for each layer. The initial value for the SiO_2 layer is based on thickness measurements during the e-beam deposition from the quartz crystal resonator. The mica thickness is based on control measurements for the same thickness of mica without the SiO_2 layer.
4. Estimated or known refractive index (RI) (minimum, maximum) for each layer. For example the known refractive index of silver (n=0.05) is used. However, mica is a natural mineral whose refractive index can vary slightly between samples and is thus fit.
5. Because of the large number of fitting parameters, the phase space is restricted by maximum and minimum values based on known physical parameters. The smallest sum of square error (SSE) between the measured FECO wavelengths and the MMM calculated FECO wavelengths is chosen to obtain thicknesses and RI of the various layers. In all cases, the SSE was «1.

To observe and measure the FECO wavelengths, we utilized a SpectraPro-¾ meter spectrometer with an integrated Princeton SPEC-10:2K Digital CCD camera. Figure 1 shows an example CCD image for 1028Å thick SiO_2 on 4.4μm thick mica. Figure 2 illustrates the intensity spectrum as a function of wavelength for a FECO image. Peak wavelength positions are obtained with Igor Pro using the Multi-peak Fitting analysis package.

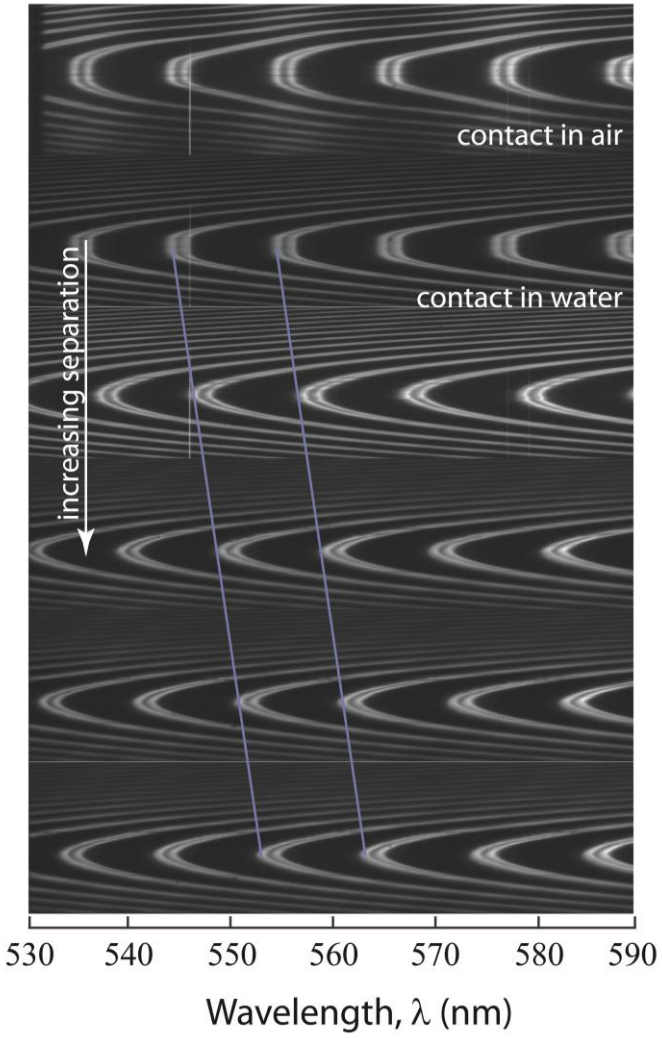

Figure 1. FECO images obtained from SFA measurements between SiO_2 coated mica surfaces in air and water.

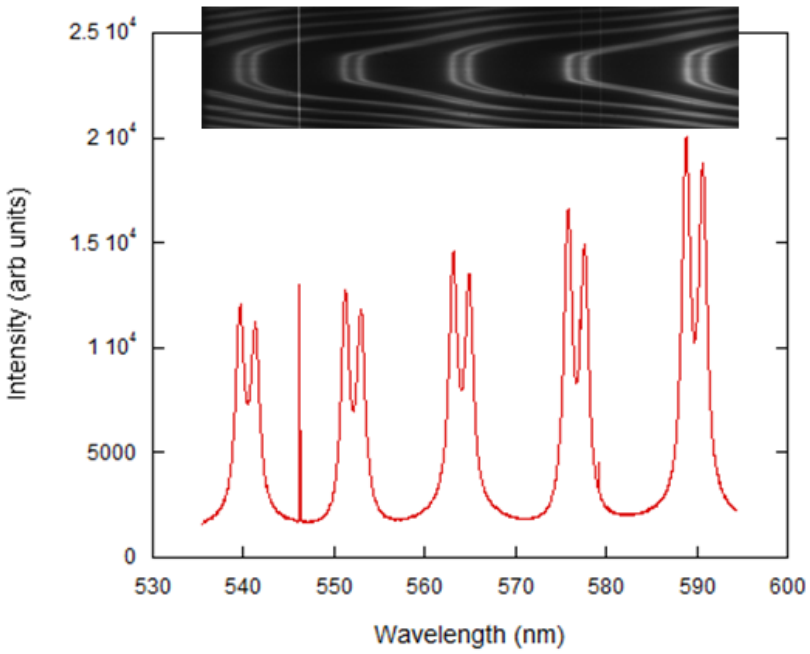

Figure 2. Simultaneous peak position and intensity of CCD captured FECO.

Analysis procedure:

For completeness, we have included the MMM equations taken directly from literature and programmed in our in-house algorithm. The characteristic matrix for an interferometer consisting of L layers can be written as:

$$\bar{M} = \prod_{j}^{L} \bar{M}_j = \begin{bmatrix} m_{11} & m_{12} \\ m_{21} & m_{22} \end{bmatrix} \tag{1}$$

Where the characteristic matrix for each layer, j, is:

$$\bar{M}_j = \begin{bmatrix} \cos\left(\frac{2\pi \bar{u}_j D_j \cos\theta_j}{\lambda}\right) & -\left(\frac{i}{\bar{u}_j \sqrt{\varepsilon_0}}\right) \sin\left(\frac{2\pi \bar{u}_j D_j \cos\theta_j}{\lambda}\right) \\ -i\bar{u}_j \sqrt{\varepsilon_0} \sin\left(\frac{2\pi \bar{u}_j D_j \cos\theta_j}{\lambda}\right) & \cos\left(\frac{2\pi \bar{u}_j D_j \cos\theta_j}{\lambda}\right) \end{bmatrix} \tag{2}$$

the transmission coefficient is expressed as:

$$t = \frac{2\bar{u}_0\sqrt{\varepsilon_0}}{(m_{11}+m_{12}\bar{u}_0\sqrt{\varepsilon_0})\bar{u}_0\sqrt{\varepsilon_0}+m_{21}+m_{22}\,\bar{u}_0\sqrt{\varepsilon_0}} \quad (3)$$

and the transmittivity is:

$$\mathrm{T} = t \times t^* \quad (4)$$

Here D_j and $\bar{u}_j$ are the thickness and the complex refractive index of layer *j,* respectively. $\bar{u}_0$ is the refractive index of the medium surrounding the interferometer, θ_j is the angle of incidence on layer *j*, ε_0 is the permittivity of space, λ is the wavelength of incoming light. If thickness, D_j, and refractive index, u_j, for each layer are known, the intensity of the transmitted light can be calculated at a given wavelength. The wavelengths at maximum transmittivity correspond to the wavelengths for each FECO.

The following are the detailed steps taken to obtain Ag, Mica, SiO_2 and bilayer thickness and refractive index for a given experiment. First, the simplest case of Silver-Mica-Silver is used to determine the mica and silver thickness and refractive index of mica. Thermal evaporation is used to deposit silver on a clean piece of mica, and the thickness of the deposited film from the quartz resonator is used as a first guess of the silver thickness (e.g. 550±50Å). The value for the refractive index of silver over the visible spectrum is, η_{Ag}=0.05.[10] The wavelength spacing of the FECO is used to provide an estimate of the mica thickness. The mica used in these experiments is ruby muscovite which provides an initial guess of refractive index η_{mica}=1.58. The silver and mica

thickness and refractive index of mica are obtained based on the smallest SSE in fitting the experimentally measured FECO positions simultaneously using a 3-layer MMM.

After determining the layer parameters for mica and silver, the thickness and refractive index of SiO_2 is determined utilizing a 5-layer MMM: Ag-Mica-SiO_2-Mica-Ag, as shown in Figure 3. As described in Materials and Methods section, SiO_2 is deposited uniformly[11] on mica via e-beam deposition. At this point, the only unknowns are the SiO_2's refractive index and thickness.

MBI analytical solution of the 3-layer and 5-layer interferometers

3-layer interferometer: consider the case where a transparent film of thickness T and refractive index u_2 is sandwiched between two symmetrical films of thickness D_1 and refractive index u_1, see Figure 3 for illustration. The analytical solution to obtain the gap thickness, T or $2D_2$, between the symmetrical films is the following[2]:

$$\tan(ku_2T) = \frac{2\bar{u}\sin\left(\frac{n\pi\Delta\lambda_n}{\lambda}\right)}{(1+\bar{u}^2)\cos\left(\frac{n\pi\Delta\lambda_n}{\lambda}\right)\pm(\bar{u}^2-1)} \quad (5)$$

Where $\bar{u} = u_1/u_2$, n is the order of interference or fringe order of the nth fringe, $k = 2\pi/\lambda$, and $\Delta\lambda_n = \lambda_n - \lambda_n^0$. The reference wavelength, λ_n^0, is obtained from the position of the n^{th} fringe when T = 0. With this method, the only unknowns are the thickness, T, and refractive index μ_2.

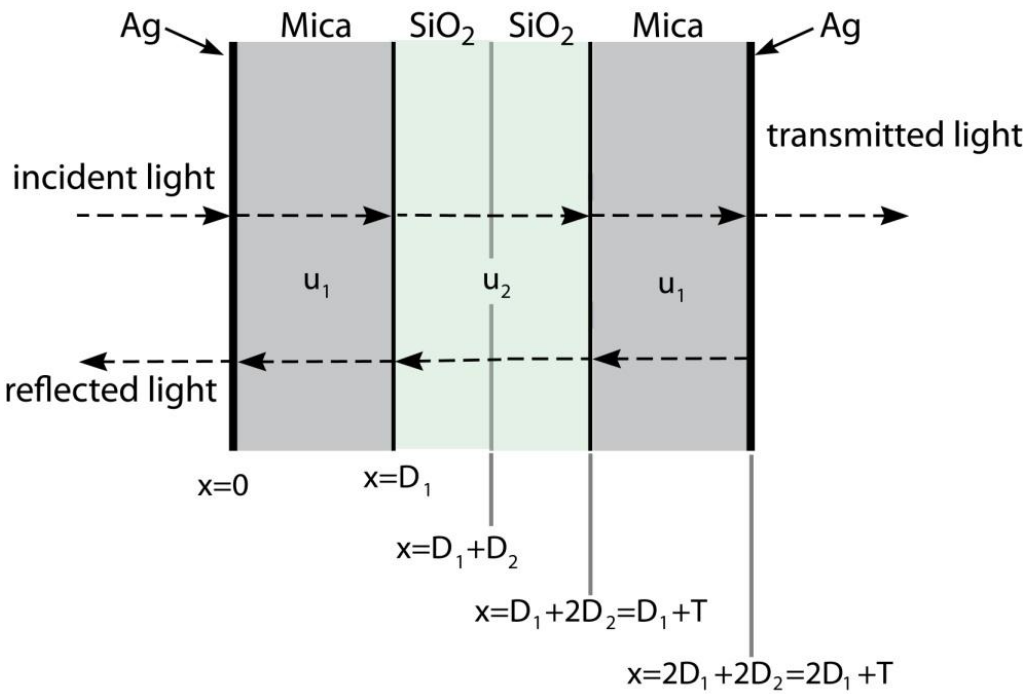

Figure 3. 3-layer interferometer used in MMM to extract SiO_2 thickness and its refractive index. This is also considered a 3-layer interferometer in MBI. Ag provides a reflective coating at x=0 and $x=2D_1+2D_2$. D_1 is the mica thickness; D_2 is the SiO_2 thickness on each side, where $2D_2=T$; u_j is the refractive index of each layer and x is the direction of the light

5-layer interferometer: consider the interferometer depicted in Figure 4, where the SiO2 films are now separated by a water film of thickness T and refractive index μ_3. The general solution for a 5-layer symmetrical interferometer is the following[2]:

$$\tan(ku_3\mathrm{T}) = \frac{(1-r_1^2)\{\sin 2k\,(u_2D_2+u_1D_1)-2r_2\sin(2ku_2D_2)+r_2^2\sin 2k(u_2D_2-u_1D_1)\}}{2r_1\{1-2r_2\cos(2ku_1D_1)+r_2^2\}-(1+r_1^2)\{\cos 2k(u_2D_2+u_1D_1)-2r_2\cos(2ku_2D_2)+r_2^2\cos 2k(u_2D_2-u_1D_1)\}} \quad (6)$$

Where $r_1=(u_2-u_3)/(u_2+u_3)$ and $r_2=(u_1-u_2)/(u_1+u_2)$. To find the water gap thickness in this case, all other parameters should be known. The refractive indexes should be established and D_1 and D_2 must be determined separately before T can be obtained, namely when T=0.

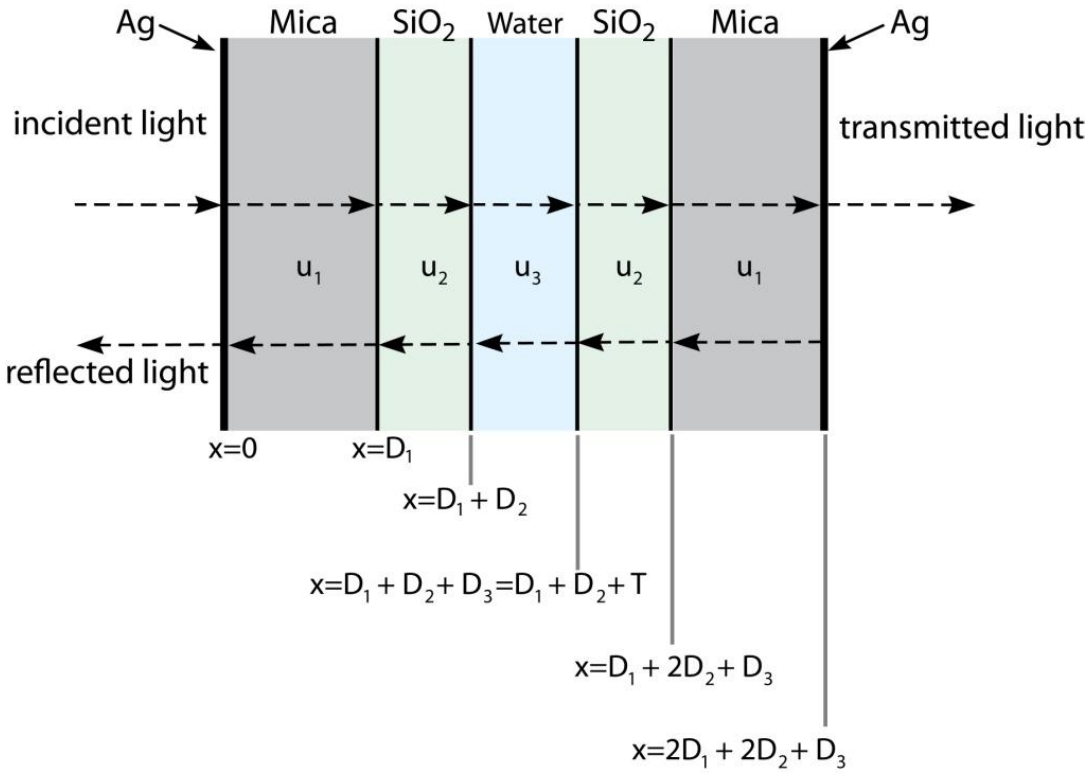

Figure 4. A symmetrical 5-layer interferometer, also considered a 7-layer interferometer in MMM. D_1, D_2, D_3 are the mica, SiO_2, and water thickness respectively. u_1, u_2, and u_3 are their refractive indexes

Results and Discussion

SiO_2 layer properties

In the original work on e-beam deposited SiO_2 films on mica, Vigil et al.[11] found that the SiO_2 films swell with humidity and reach a maximum and constant thickness in

water. The change in thickness was reported to be ~20Å, in agreement with our experiments, see Table 1 for experimental results.

Table 1. SiO_2 thickness in air vs. water

	Thickness (Å)	RI	SSE
Quartz Crystal Reading	1000	--	--
In air using MMM	1028	1.46	0.0852
In water using MMM	1051	1.46	0.0042

The uniformity of the SiO_2 thickness and RI underwater was determined by measuring contact between the films in water at various locations. Table 2 lists the thickness, RI, and SSE values obtained using MMM for multiple experiments. In all cases, the minimum SSE was obtained with a refractive index of 1.46 for the SiO_2 film in agreement with ellipsometer measurements and other literature values[11].

Table 2. Comparing SiO_2 thickness using quartz crystal and MMM. The measurements are of SiO2 surfaces in hard contact under water.

	SiO_2 Thickness from the Quartz Crystal Reading	SiO_2 Thickness in water using 3-Layer MMM (Å)	SiO_2 RI	SSE
Experiment A	1000	1051-1053	1.46	0.004+0.05
Experiment B	530	581-587	1.46-1.47	0.049+0.05
Experiment C	500	527-531	1.46-1.47	0.018+0.09

Comparison between 7-layer MMM and analytical solutions of MBI

One of the most significant differences between MMM and the analytical MBI methods is that MBI provides a simpler and more efficient way to analyze data. The analytical 5-layer solution is comparable with the 7-layer MMM, thus we are interested in

determining the error in approximating a 7-layer MMM with a 5-layer and 3-layer MBI solution.

Consider the case where a water layer is in between SiO_2-covered mica surfaces and the system is symmetrical, see Figure 4 for illustration. To compute the water gap thickness (T), all other parameters in equations (5) and (6) must be established. To utilize the analytical 3-layer MBI solution for a 5-layer interferometer, we decided to combine the mica and SiO_2 layers into one with a joint thickness and refractive index.

In Table 3, we tabulate the calculated water thickness at different separations for all methods of analysis. We also included the % difference between MMM and MBI.

Table 3. Water thickness at different separations using MMM and BMI. The reference for MBI was SiO_2 contact in water.

Water Thickness (Å)				
MMM	3-Layer MBI	%Difference btw MMM and 3-Layer MBI	5-Layer MBI	%Difference btw MMM and 5-Layer MBI
0	0	----	0	----
196	171	12.8	190	3.4
402	363	9.7	403	0.3
836	783	6.3	862	3.0
1283	1232	4.0	1324	3.1
1672	1636	2.2	1712	2.3

As shown, the 3-layer MBI provides a good starting estimate for the separation distance for the MMM analysis. Although the SiO_2 thickness is relatively small compared to the base mica substrates (~2% of mica thickness), it has a significant impact in the calculated separation distance when the system is approximated using only a 3-layer model. The 5-layer model, on the other hand is in very good agreement with MMM.

Conclusion

In this work, SFA was used to obtain experimental data gathered from the FECO peak positions captured using a CCD camera. Here, we showed that for a 5-layer system (Figure 4), it is insufficient to use the 3-layer for analysis and can only serve as a first approximation to measure separation distance between surfaces. It was observed that for separation distances less than 200Å, there is a ~13% difference between the MMM and the 3-layer analytical method, whereas there is only a ~3.5% difference between the MMM and the 5-layer analytical method. For distances higher than 1000 Å, however, the difference between MMM and any analytical methods converges, making any of these methods employable to obtain large distances between surfaces.

References

1. Leckband, D.; Israelachvili, J., Intermolecular forces in biology. *Quarterly Reviews of Biophysics* **2001,** 34, (2), 105–267.

2. Israelachvili, J., Thin film studies using multiple beam interferometry. *J. Colloid Interface Science* **1973,** 44, 259.

3. Israelachvili, J. N., and Adams, G. E., Measurement of Forces between Two Mica Surfaces in Aqueous Electrolyte Solutions in the Range 0-100 nm. *Chem. Soc., Faraday Trans.* **1978,** 74, 975-1001.

4. Orozco-Alcaraz, R. K., T.L. , Impact of membrane Fluidity on Steric Stabilization by Lipopolymers. *Langmuir* **2012,** 28, 7470-7475.

5. Moore, W. N. a. K., T.L., The role od flexible tethers in multiple ligand-receptor bond formation between curved surfaces. *Biophysical Journal* **2006,** 91, (5), 1675-1687.

6. Born, M. W., E., *Principles of Optics*. Pergamon Press: London, 1959.

7. Clarkson, M. T., Multi-beam interferometry with thin metal films and unsymetrical systems. *Applied Physics* **1989,** 22, 475-482.

8. Heuberger, M. L., G.; Israelachvili, J., Topographic Information from Multiple Beam Interferometry in the Surface Force Apparatus. *Langmuir* **1997,** 13, 3839-3848.

9. Mangipudi, V. S., Analysis and Application of a 5-Layer Multiple Beam Interferometer in the Surface Forces Apparatus. *Colloid and Interface Science* **1995,** 175, 484-1995.

10. Levins, J. M. V., T.K., Reduction of the Roughness of Silver Films by the Controlled Application of Surface Forces. *The Journal of Physical Chemistry* **1992,** 96, (25), 10405-10411.

11. Vigil, G. X., Z.; Steinberg, S.; Israelachvili, J., Interactions of Silica Surfaces. *Colloid and Interface Science* **1994,** 165, 367-385.

CHAPTER 2

Interaction forces between DPPC bilayers on glass

Adapted with permission from Raquel Orozco-Alcaraz and Tonya L. Kuhl. Impact of membrane fluidity on steric stabilization by lipopolymers. *Langmuir*, **2012**.

Abstract

The Surface Force Apparatus (SFA) was utilized to obtain force-distance profiles between silica supported membranes formed by Langmuir-Blodgett deposition of 1,2-dipalmitoyl-*sn*-glycero-3-phosphocholine (DPPC). In the absence of a membrane, a long range electrostatic and short range steric repulsion is measured due to deprotonation of silica in water and roughness of the silica film. The electrostatic repulsion is partially screened by the lipid membrane and a van der Waals adhesion comparable to that measured with well packed DPPC membranes on mica is measured. This finding suggest that electrostatic interactions due to the underlying negatively charged silica are likely present in other systems of glass supported membranes. In contrast, the charge of an underlying mica substrate is almost completely screened when a lipid membrane is deposited on the mica. The difference in the two systems is attributed to stronger physisorption of zwitterionic lipids to molecularly smooth mica compared to rougher silica.

Introduction

Due to the complexity of cell membranes, biophysical studies have primarily focused on model membrane systems of reduced complexity in order to elucidate the fundamental thermodynamics and physics of membrane interactions. For example, lipids and their self-organizing structures have been broadly used as models of cellular membranes and studied for their potential in biosensor applications[1]. In this work we compare the interaction forces between supported membranes composed of one of the

most commonly studied phospholipids, DPPC on two different supports; molecularly smooth but chemically inert mica versus more functional and broadly used silica or glass.

There are a plethora of techniques used to study membranes, however relatively few provide a measure of membrane-membrane interactions[2-3]. One of the first methods developed relied on changes in the spacing between membranes in multilamellar stacks under osmotic stress to extract the repulsive interactions between membranes[4-5]. Such studies provided unprecedented understanding of the role of membrane undulations and hydration. The use of small and wide angle x-ray and neutron scattering also provided high resolution density distributions and average packing of lipids in the membrane to be obtained.[6-9] More recently, the bioforce probe based on micropipette aspiration of giant unilamellar vesicles has been used to measure membrane-membrane interactions. Initially used to study membrane tension and area compressibility by measuring changes in membrane shape as a function of pipette suction pressure, the use of opposing membranes and/or a force sensing red blood cell expanded the measuring capability to detect weak attractive interactions as well as biological specificity interactions such as ligand-receptor binding[2, 10-12]. In terms of substrate supported membranes, Atomic Force Microscopy (AFM)[13] is widely used to measure membrane topology, but only sparingly used to measure membrane-membrane interactions due to challenges in forming a membrane on silicon nitride tips.[14-16] Chemically functionalizing the tip with gold and a hydrophobic mercapto undecanol has been shown to promote spontaneous vesicle fusion, yielding a supported lipid monolayer appropriate for measuring membrane-membrane interactions.[15]

The most widely used and versatile technique for measuring membrane-membrane interactions is the Surface Force Apparatus, which provides force-distance profiles with 1Å resolution in distance, 10pN in force, and visualization of the area of contact between two macroscopic membrane coated surfaces.[2, 17-22] Traditionally, SFA employs mica, a molecularly smooth and widely used solid support for force spectroscopy and fluorescence microscopy measurements. However, membrane based biosensors typically use silica or glass substrates; in part due to the fact that silica is readily available, cheap, easily chemically modified, optically transparent, and less sensitive to surface damage[23-25]. It is, thus, important to establish the typical conditions present (e.g. charge density, hydrophobicity, steric interactions, etc.) for a bilayer immobilized on silica and thus how a silica supported membrane interacts with materials in the environment (e.g. particles, proteins, cells, etc.) for applications. Moreover, there is a large effort to develop models to recapitulate integral membrane proteins in supported membranes for controlled biophysical studies[26-28]. In order to study the interaction of membranes with transmembrane proteins, it is necessary to prevent deleterious interactions of the embedded protein with the underlying inorganic support. Hydrophilic polymer cushions are actively being pursued as a means to provide a highly hydrated, soft, flexible spacer between the substrate and the membrane to better mimic biological conditions and native function [24, 29-40] Grafting of polymers on silica is becoming routine. Follow on work will present studies of interaction forces of polymer cushioned membranes.[41]

Though the interaction between lipid bilayers immobilized on mica surfaces have been well documented, no work has reported measurements of membranes immobilized

on silica using the SFA. In this work, we measure and analyze the interaction between two DPPC bilayers deposited on smooth silica thin-films. The silica (SiO_2) is deposited via electron beam deposition (e-beam) on mica to yield relatively smooth films (5Å rms). The resulting optical interferometer is analyzed using both the 5-layer multiple beam interferometry analytical solution and multiple matrix solution of the full optical system (see Chapter 1). The results are compared to the interaction of bilayers immobilized directly on mica under similar conditions.

Materials and Methods

Chemicals.

1,2-dipalmitoyl-*sn*-glycero-3-phosphocholine (DPPC) (melting point 41°C) was purchased from Avanti Polar Lipids, Inc. (Alabaster, AL). Texas Red® 1,2-Dihexadecanoyl-sn-Glycero-3-Phosphoethanolamine, Triethylammonium Salt (TexasRed DHPE) was purchased from Life Technologies Corp. (Grand Island, NY). Lipids were dissolved in chloroform at a concentration of 1 mg/ml. KNO_3 was used as the monovalent electrolyte in all solutions. The water used was purified with a MilliQ Gradient water purification system, with a resistivity of 18MΩ·cm.

Sample preparation.

Silica-covered mica was prepared based on the procedures previously described by Vigil et al.[42] First, mica was cleaved to uniform thicknesses of 3 to 4 microns, and adhered to a clean mica backing sheet. A CHA e-beam evaporator SEC-600-RAP was then used to deposit SiO_2 onto the mica pieces. To ensure uniform deposition the

samples were rotated in their planetaries and the raster was scanned at an amplitude of one fourth of the crucible's diameter. Films with approximately 500Å or 1000Å SiO_2 layers were deposited using the following operating conditions; base pressure of 10^{-6} torr, deposition pressure of $5x10^{-6}$ torr, filament current of 26mA, accelerating voltage of -10kV, and a deposition rate of ~1Å/s. After the SiO_2 was deposited, the SiO_2-covered mica pieces were flipped and adhered to a clean mica sheet and silver was evaporated onto the backside of the mica pieces. Samples were stored under vacuum in this configuration until use.

Supported lipid bilayers were prepared by Langmuir-Blodgett (LB) deposition using a temperature-controlled Wilhelmy Trough (Nima Coventry, UK) and assembled onto the back-silvered mica or SiO_2 covered mica substrates glued onto cylindrical silica disks, a procedure described elsewhere.[43-44] Prior to lipid deposition the SiO_2-mica surfaces were placed under UV light for a total of 30 minutes in 10 minute increments to ensure cleanliness and surface hydroxylation. Both the inner and outer leaflets of DPPC were deposited at 45mN/m. The inner leaflet was deposited by raising the substrates vertically through a compressed DPPC monolayer at the air-water interface at a dipping speed of 1mm/min. The monolayer transfer ratio was 1.00±0.05 on mica and 0.97±0.05 on SiO_2-mica. Subsequently, the outer DPPC layer was deposited in a vertical geometry under similar conditions but at a faster deposition rate of 4mm/min to prevent desorption of the inner leaflet at the air-water interface. The transfer ratio for the outer monolayer was 1.00±0.05 on mica and 0.90±0.05 on SiO_2-mica. The pressure-area isotherms obtained were in agreement with those in literature.[45] To demonstrate the similar quality of the deposited DPPC membranes on mica and SiO_2-mica surfaces, fluorescence images

of DPPC membranes containing 1mole% Texas Red DHPE are shown in the Figure 3. No fluorescent dye was incorporated into membranes for SFA experiments.

Atomic Force Microscopy (AFM).

AFM studies were done using the NEAT-ORU spectral imaging facility at the UC Davis campus with an Asylum Research (Santa Barbara, CA) MFP-3D AFM. Veeco SiliconNitride MSCT levers, k~=0.03, were used for imaging.

Surface Force Measurements.

The SFA technique has been used extensively to measure interaction forces between surfaces[46-47]. After bilayers were deposited on the solid support, the surfaces were transferred and mounted into the SFA under water, a procedure detailed elsewhere[17]. The water in the SFA box was saturated with a speckle of DPPC to prevent lipid desorption from the substrate during the course of the measurements. After the surfaces were mounted, the SFA box was placed in a temperature controlled room at 25.0°C. A custom, automated SFA was used for convenient data collection[48]. The system enables constant and/or variable motor displacements via a computer controlled motor system. A sensitive CCD camera (Princeton SPEC-10:2K Roper Scientific, Trenton NJ) was interfaced with the spectrometer and computer acquisition system to allow automated wavelength determination of the fringes of equal chromatic order.

The separation distance analysis traditionally used for supported membranes on mica surfaces is to approximate the system as a symmetric 3-layer interferometer and use analytical solutions for the resulting optical interferometer. Other methods include a 5-

layer analytical form and the multilayer matrix model (MMM) that can be used for asymmetric and more complicated optical systems. Immobilizing bilayers on mica-covered silica surface requires an extra set of symmetric layers in the interferometer and complicates the analysis of the separation distance. In the Chapter 1 for this work, we demonstrate that approximating the optical system using a simple 3-layer interferometer is insufficient, and can only be used as a first estimate of the separation distance. The difference between the results obtained using the 3-layer analytical method and MMM is ~13%, while the difference between the 5-layer analytical method and MMM is ~3.5% for separation distances less than 200Å. In this work the 5-layer analytical method was primarily employed. Membrane thickness at contact was determined using MMM.

Results

AFM of SiO_2 covered mica.

Figure 1A shows a representative AFM image of a ~1000Å-thick SiO_2 layer, e-beam deposited on mica hydrated in MilliQ water. Figure 1B shows the 3-dimensional profile that corresponds to image 1A. Image analysis gave a peak to valley roughness of 31±2Å for a hydrated film in bulk water (6±2Å rms). Similar surface quality was observed with dry films in air (results not shown). In all cases scans were recorded over different regions of the films and the scans were reproducible. Similar, but lower, values for the roughness of e-beam deposited SiO_2 thin films on mica were reported by Vigil et al. The surface quality of our films is also consistent with SFA measurements, where we

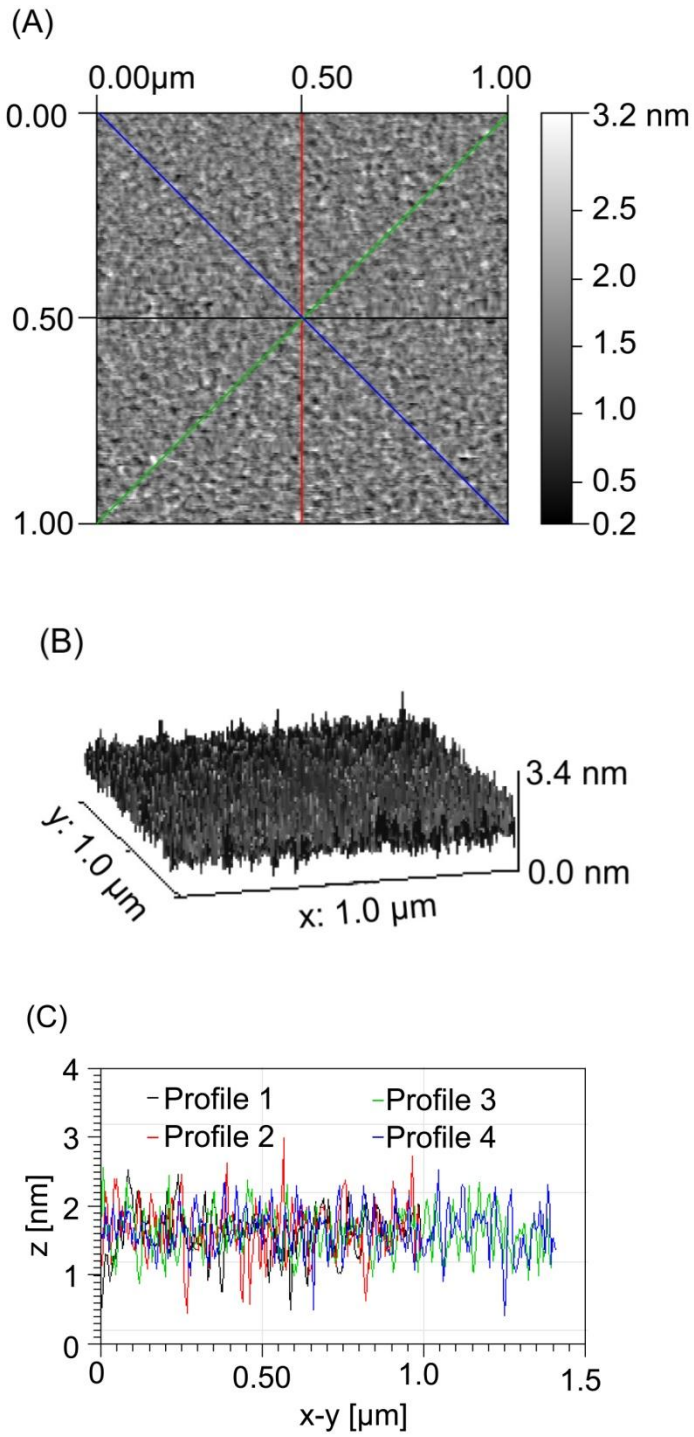

Figure 1. (A) Representative 1µm × 1µm AFM scans of a SiO_2 e-beam evaporated film on mica in MilliQ water. **(B)** 3D profile of (A). The peak to valley roughness of the film is 31±2Å. **(C)** 2D (x-y vs. z) scans of different regions of Figure 1A. The vertical line in part (A) corresponds to Profile 1, horizontal line corresponds to Profile 2, diagonal (tilted to the right) is Profile 3 and diagonal (tilted to the left) is Profile 4.

found the SiO_2 films swelled slightly by 2.2% in water compared to their dry thickness (see Chapter 1). Vigil et al. suggested the swelling was due to formation of protruding silica hairs or gel formation at the SiO_2-water interface. As the roughness of our SiO_2 film did not increase appreciably upon hydration, we attribute the 2.2% increase in film thickness to imbibing a small amount of water in defects within the SiO_2 film.

SiO_2 interaction in aqueous solution.

Figure 2 shows the force-distance profile between two e-beam evaporated silica films on mica in ~0.5mM KNO_3 at pH 6. Contact, D=0, was defined as hard flattened contact in air ($F/R \geq 70$ mN/m). The force curve is characterized by two types of repulsive interactions: the expected long range electrostatic double layer interaction due to the negative charge of the silica film in water and a shorter-range steric interaction presumably due to surface roughness and hydration[49-50]. Theoretically and experimentally both electrostatic and steric/hydration interactions decay roughly exponentially. The silica surfaces were assumed to be symmetric, ie. the films had the same negative charge density or surface potential. The electrostatic interaction was then fitted by solving the nonlinear Poisson-Boltzmann (P-B) equation using a numerical algorithm developed by Grabbe and Horn.[51] The algorithm explicitly computes the electrostatic potential or constant surface charge between two flat surfaces using a relaxation method on a finite mesh. The Derjaguin approximation was used to convert from the energy between flats to force between crossed cylinders, $F/R = 2\pi E$. The solid lines are the P-B fits for a constant potential of ψ = -107mV and a constant surface charge of $\sigma = 9.2 mC/m^2$. These results are in good agreement with previous studies where the magnitude of the negative

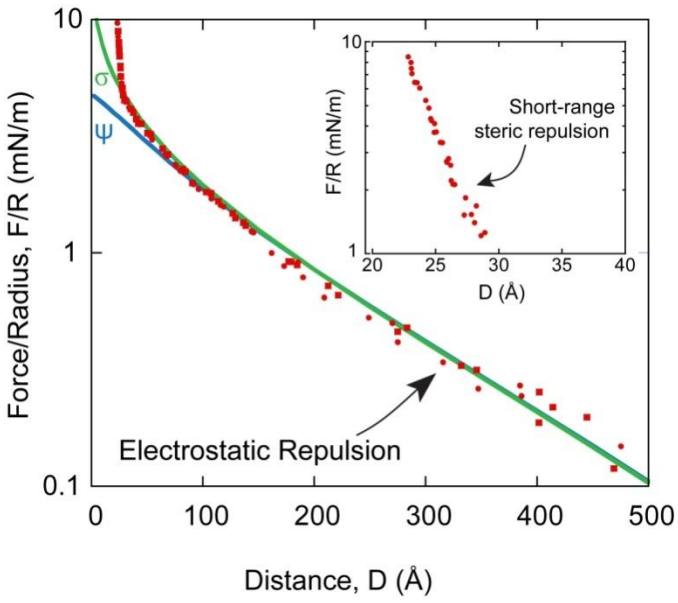

Figure 2. Force-distance profile between two e-beam evaporated silica films on mica substrates in ~0.5mM KNO_3. Solid lines are electrostatic fits to the data using the Poisson-Boltzman (P-B) equation with constant surface potential ψ= -107mV and constant surface charge σ= -9.2mC/m^2. D = 0 is defined as hard, flattened contact between the silica films (F/R>70mN/m) submerged in water. (Inset) Remaining steric force after subtracting the electrostatic contribution.

surface potential of silica at pH = 7.5 was ψ = -120mV in 0.1mM NaCl.[23, 52] For the conditions here, pH~6, a lower charge density and zeta potential are expected.[53]

To better qualify the short-range interaction, the electrostatic contribution was subtracted from the measured force profile[43]. The remaining, steric portion of the interaction is shown in the Inset of Figure 2. The measured force profile deviates from a purely electrostatic interaction at short range, D<30Å, consistent with the AFM topography measurements in Figure 1. When an exponential is fit F/R~exp (D/L_c), we find that the characteristic length for this case is L_c~6Å. The characteristic length is consistent with hydration of the silica interface and compression/interdigitation of protrusions of the opposing surfaces (6±2Å rms).[49-50] This additional repulsive

contribution can possibly be explained by Valtiner at al., who suggested that this additional force is attributed to repulsive hydration and steric forces.[54-55] After hydration, no change in the interaction profile was detected over many days demonstrating that the films were stable. A similar short-range repulsion between silica films in water was observed by Vigil et al.,[42] but attributed to the extension of dangling Si-(-O-Si-)n-OH groups and formation of a silica gel.

Fluorescent microscopy images of supported DPPC membranes on mica and silica coated mica.

Figure 3A and 3B show representative fluorescent images of LB deposited DPPC bilayers on mica and silica-coated mica containing 1 mole% Texas Red DHPE. The membranes are uniform and very similar in both cases. Small domains appear throughout the images; the uniformity confirms that a well packed membrane exists on both substrates but the resolution of the images does not allow differentiating between the two. Fluorescence recovery after photobleaching (FRAP) measurements were performed to confirm the gel phase state of the DPPC membrane at room temperature. FRAP has been used extensively to measure the lateral diffusion coefficient of model membranes.[56-58] A small area was photobleached with high power light, leaving behind a dark circular region (as seen in Figure 3A and 3B). When the bilayer is in the fluid phase, diffusion drives the lipid components, along with the integrated fluorophore, into/out-of the bleached area leading to a recovery of the bleached spot. No recovery over an hour time scale was observed (Figure 3A and 3B), which is expected for DPPC at 25°C.

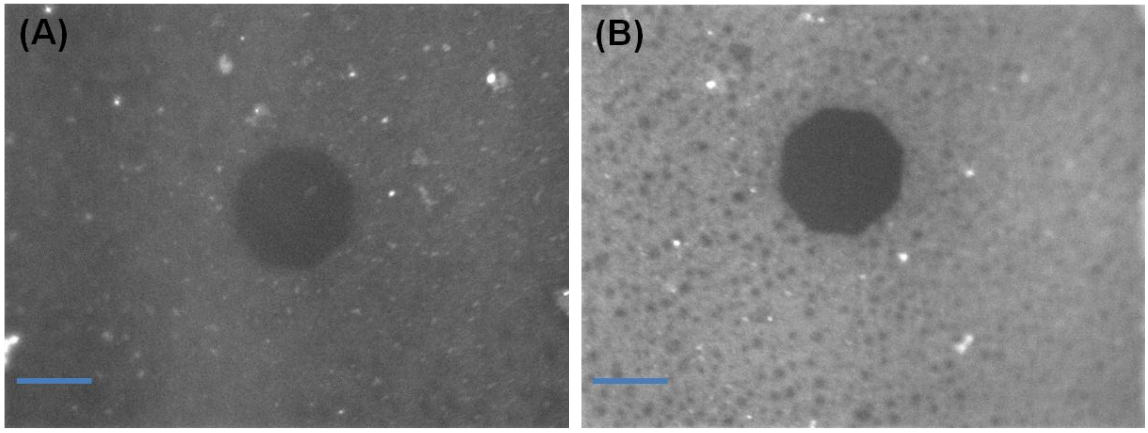

Figure 3. Fluorescent images of DPPC bilayers + 1% Texas Red DHPE deposited via LB deposition at room temperature. **(A)** Bilayer on mica. **(B)** Bilayer on e-beam deposited SiO_2-covered mica. Horizontal line represents 20μm

Control measurements of DPPC bilayers on mica.

Traditionally DPPE has been used as the inner leaflet layer in supported membrane experiments measured with the SFA. DPPE binds to mica through a strong electrostatic interaction and provides a stable hydrophobic surface upon which to deposit the outer lipid monolayer leaflet. Here, a symmetric DPPC bilayer was used instead as DPPC is one of the most commonly studied phospholipids and considered a better mimic of biological membranes.[23, 59] Before describing the results of the force-distance, F(D), measurements, it is important to establish an appropriate reference frame for the contact between the bilayer surfaces, which will define D=0. As in previous SFA measurements, we choose to define D=0 as contact between the membranes in the absence of hydration and protrusion effects.[17] In the case of DPPC membranes supported on mica, the hydrated thickness of the two outer monolayers, Δ, was determined at the end of each experiment by measuring the thickness change following drainage of the solution from the apparatus and removal of the two outer monolayers. From the measured thickness

change relative to contact between the bilayers at a force of about 10mN/m, bilayer-bilayer contact, D=0, was defined as

$$D = \Delta - T \quad (1)$$

The anhydrous bilayer thickness (T) was calculated from the known volumes occupied by the hydrocarbon chains and PC head group given by

$$T=2[2V_{hc}+ V_{head}]/A \quad (2)$$

where $V_{hc} =(27.4 + 26.9n)\ Å^3$ is the average volume of a saturated n-carbon chain in the gel state[60], V_{head} = 324.5Å^3 is the average head group volume of PC[61], and A is the deposited area per lipid. For example, the thickness of two outer DPPC monolayers deposited at A = 48 Å^2 per molecule (Π=45mN/m) is T = 2[2(27.4 + 26.9x15) + 324.5]/48 = 49.4Å. Typically, phosphotidylcholine membranes come into contact at separations of about 20-30Å depending on the compressive load.[17, 62] The thickness of the bilayer was assumed to remain constant during experiments. This is reasonable given that the DPPC monolayers (T_{mp} = 41°C) were deposited at room temperature in a close packed solid phase and no phase changes or density changes are expected to take place.

Figure 4A shows the measured force-distance profile between two DPPC bilayers immobilized on mica substrates in a monovalent solution of 0.5mM KNO_3 at room temperature. As can be seen, a very weak repulsion[63] is observed between the surfaces for separations below ~150Å followed by a strong, short-range repulsion at about 30Å. As DPPC is zwitterionic, but overall neutral, we attribute the weak repulsion to a small level of residual charge from the mica surfaces or lipid membrane as the decay length is roughly consistent with the electrolyte concentration[63]. If fully dissociated, mica has a maximum surface charge density[46] of 50Å^2/e$^-$. The surface charge density or surface

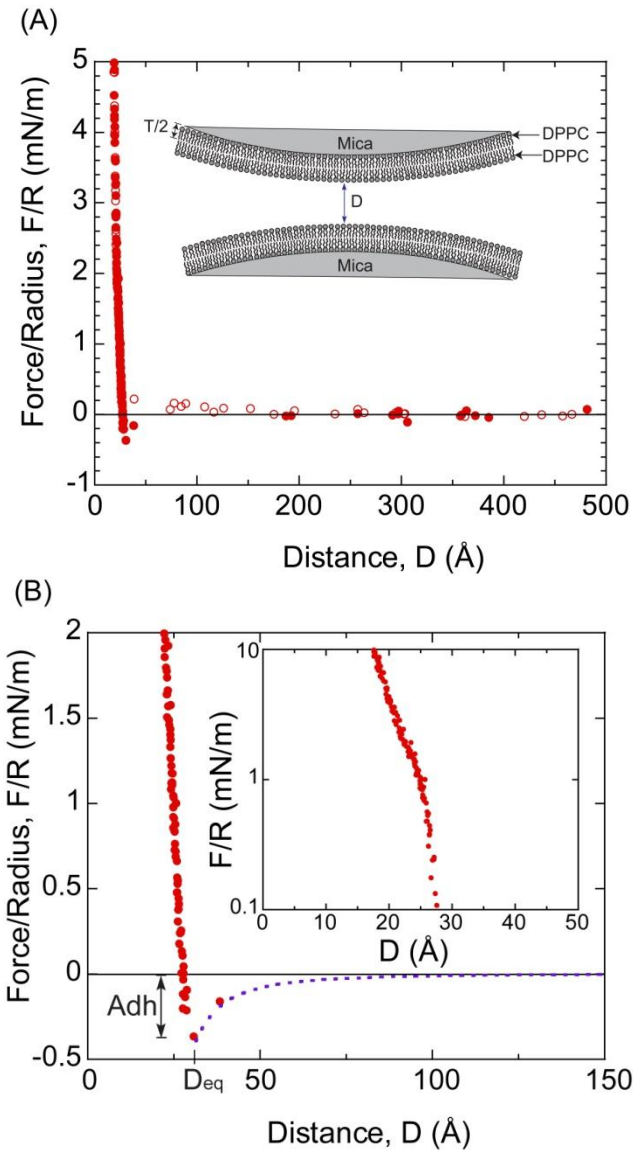

Figure 4. **(A)** Force-distance profile between two DPPC bilayers supported on mica in a monovalent solution of 0.5mM KNO_3. Open circles indicate approach and closed circles indicate separation. (Inset) Illustration of the two DPPC membranes on mica, where D=0 is defined as the contact between two non-hydrated DPPC bilayers. T is the thickness of a DPPC leaflet. **(B)** Small range plot of the data in (A) showing the van der Waals interaction $F= -AR/6D^2$ (dash line) with $A=(7\pm1)\times10^{-21}$J. A_{dh} is the magnitude of adhesion force. (Inset) Semi-log plot of the repulsive portion of the force profile.

potential measured experimentally is dependent upon the type and concentration of electrolyte present in the solution. As shown in Figure 3A, the surface charge of the mica is almost completely damped after depositing a bilayer (with a low dielectric oil core) on the surface.[64] The almost-negligible electrostatic repulsion suggests reasonably strong electrostatic binding of DPPC lipid bilayer to mica. The electrostatic binding rises from the attractive interaction between the underlying, negatively charged mica substrate and the positively charged terminus of the zwitterionic headgroup. In contrast, no electrostatic repulsion is measured when the inner leaflet of the membrane is DPPE. Presumably the difference resides in the weaker physisorption and higher hydration of PC headgroups compared to PE headgroups[65].

Figure 3B illustrates the van der Waals adhesion between the DPPC bilayers with a magnitude of $A_{dh} = F_{ad}/R = -0.40 \pm 0.10$ mN/m at a separation of $D = 30 \pm 3$Å. In addition, the experimental data was compared to the theoretical Van der Waals interaction[17] $F=-AR/6D^2$ (dash line) with $A=(7\pm1)\times10^{-21}$J, with excellent agreement. The inset in Figure 3B is a semi-log plot of the short range repulsion between the membranes. An ever present hydration layer on the head groups and the thermal protrusions of lipids from the membrane are responsible for the short range repulsion. In addition, as suggested Marra and Israelachvili[17], the hydration of cations can also add to the repulsive force.

SFA measurements of DPPC bilayers immobilized in SiO_2

The measured transfer ratio of DPPC bilayer on the SiO_2 coated mica surfaces was 0.97±0.05 for the inner leaflet and 0.90±0.05 for the outer leaflet. This result

corroborates an earlier reflectivity studies that showed the formation of a well packed membrane with near complete coverage on a silica surface using the LB deposition technique.[66] Fluorescence images of DPPC membranes containing 1mole% Texas Red DHPE on SiO_2 coated mica are shown in Figure 3. As evidenced by fluorescence microscopy well packed membranes are present at the micron scale. However, the presence of small defects cannot be ruled out from such measurements. The lower transfer ratios of lipid monolayers obtained on silica to mica also suggest that the membranes on silica contain a higher number of defects, which is consistent with the significant electrostatic repulsion measured with silica supported DPPC membranes described in the next section. Bassereau and Pincet demonstrated that lipids in the inner leaflet can desorb during the deposition of the outer leaflet monolayer, thereby resulting in lower transfer ratios and holes in the bilayer. The holes span the thickness of the bilayer due to the high energy of exposing hydrophobic chains to water. The adsorption energy of a DPPC lipid to SiO_2 vs mica can be readily estimated from their transfer ratios using:[67]

$$E_a/kT = (\alpha\, a_m\, \gamma_{DPPC}/kT) - ln(\rho) \qquad (3)$$

where E_a is the adsorption energy, k is the Boltzmann's constant, T is the temperature, a_m is the molecular area of DPPC (a_m= 45 Å^2 at Π_{DPPC} =45mN/m),[68-69] α is a correlation coefficient, and γ_{DPPC} is the surface tension of DPPC at the air-water interface defined as γ_{DPPC} = 72mN/m -Π_{DPPC}.[70] The ratio between the total surface covered by holes and bilayer is $\rho = x/(1-x)$, where x can be found from the transfer ratio, x =(1-R)/2.[67] To calculate the adhesion energy, we assume α=0.7, the correlation value measured for DMPE on mica[67]. This yields an adsorption energy of a DPPC bilayer on silica of E_a~

$1kT$ (for R=0.90) vs. an adsorption energy on mica of $E_{a,min} \sim 3kT$ (for R=0.99). This difference confirms the lower adsorption energy of DPPC bilayers on silica than mica.

Figure 5A shows the measured force-distance profile of DPPC bilayers immobilized on silica substrates under different ionic strengths (0.5 and 1.5mM KNO_3). The reduction of the long-range repulsion with increased salt concentration clearly demonstrates that the interaction is electrostatic. As mentioned earlier, the head groups of the lipid bilayers are zwitterionic but overall neutral in charge. Thus, the long range electrostatic force is due to the underlying, negatively charged SiO_2 coated mica substrates. To clearly delineate the electrostatic contribution of the SiO_2 films in the measured force profile, the reference frame, D=0, is based on SiO_2-SiO_2 contact in 0.5mM KNO_3 aqueous solution rather than DPPC-DPPC membrane contact. The distance-shift was based on the contact before (SiO_2-SiO_2 in water) and after the bilayers were immobilized on silica using MMM to determine the thickness of the membranes. MMM was used in this case to ensure correct membrane thickness measurements. Equation 1 was also employed to observe consistency in outer layer thickness between immobilized bilayers on silica vs. mica. Interestingly, we observed an additional shift of 20Å in the thickness estimated by draining the SFA of water and removal of the outer DPPC monolayer leaflets compared to studies on mica. We attribute this to some loss of the inner layer leaflets of the membranes immobilized on silica. Removal of more than the outer two leaflets demonstrates a weaker physisorption of the inner leaflet to silica as compared to mica again consistent with the difference in the estimated adsorption energy (Eq. 3).

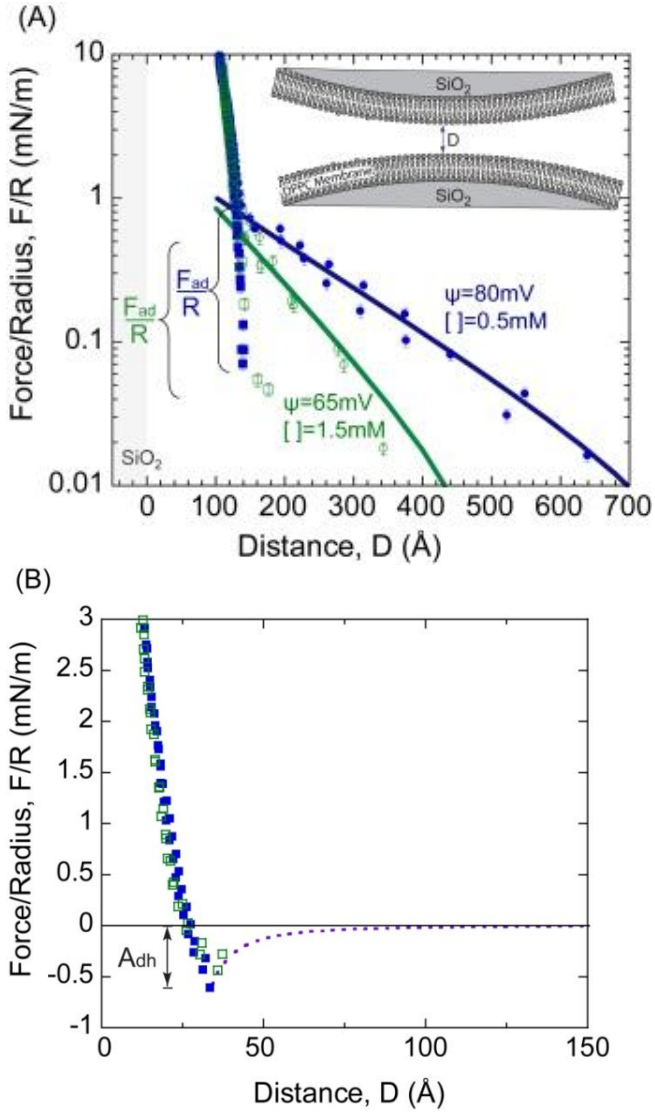

Figure 5. (A) Measured force profile between DPPC-DPPC membranes supported on SiO_2–covered mica in 0.5mM and 1.5mM KNO_3. D = 0 is defined as contact between bare SiO_2-SiO_2 surfaces in 0.5mM KNO_3. **(B)** Force profile after the electrostatics have been subtracted from the measured force profile in (A). D=0 is based on the contact between two dehydrated DPPC bilayers. Dash line is the theoretical Van der Waals fit ($F=-AR/6D^2$). $A_{dh} = F_{ad}/R$ is the magnitude of the adhesion force.

The electrostatic repulsion was fit using the Poisson-Boltzmann (P-B) equation at the two salt concentrations. The electrostatic potential decreases slightly as the electrolyte concentration increases, and the potential is lower in the presence of a membrane (Figure 2). The significant electrostatic repulsion is likely due to small holes in the membrane, and therefore, less screening of the underlying substrate charge by the supported membrane. Adhesion is again observed when the surfaces are separated. The adhesion is comparable between the two salt concentrations with a magnitude of about -0.65mN/m. This is in very good agreement with the expected VDW adhesion between DPPC bilayers.[17] No additional attraction or adhesion from hydrophobic interactions was detected. This is consistent with the formation of membrane spanning holes as observed by AFM[67, 71-72]. We further comment that the measured adhesion is identical to the measured adhesion of DPPC membranes on mica once the small electrostatic contribution is accounted for, -(0.40+0.20)mN/m.

After subtracting the electrostatic contribution (Figure 5B) the remaining short range repulsion is "softer" compared to when the bilayer is supported on mica substrates. This softer repulsion is consistent with the increase in surface roughness.[54-55] For this figure, D=0 was defined as the contact between DPPC bilayers for ease of comparison to data shown in Figure 4. To obtain D=0, the thickness of two DPPC membranes was determined using Equation 2 and subtracted from the total thickness as determined using MMM and the contact wavelengths in the presence and absence of the membranes.

Conclusions

Though the interaction between lipid bilayers immobilized on mica surfaces have been well documented, much less work has been done on bilayers immobilized on silica. The closest system was a measurement of a lipid bilayer on mica with a bare silica surface by Anderson et al.[23] The measured profile between a mica supported membrane and bare silica surface demonstrated that a long range repulsion force, attributed to residual double layer potential, and short-range repulsive thermal undulation forces were the dominant interactions.

The structure of DPPC membranes is similar on mica or silica surfaces as ascertained by fluorescence microscopy (Figure 3), however it is likely that silica supported membranes contain more holes as indicated by reduced transfer ratios.. The measured forces between DPPC bilayers immobilized on silica or mica are also similar, with the exception of a stronger electrostatic repulsive force present when silica is used. A summary of the forces and observations made in these experiments is enumerated next. First, the most important difference between the interaction of bilayers immobilized on mica and bilayers immobilized on silica is the presence of a strong electrostatic force when silica is used. We attribute this force to holes in silica supported membranes due to the weaker physisorption of lipids to the silica substrate and the hydrated surface roughness of the silica. These defects are below the resolution of fluorescence microscopy. Second, a van der Waals attraction consistent with well-packed membranes is measured upon membrane separation. In Figure 4B and 5B, the theoretical Van Der Waals interaction, $F=-AR/6D^2$ with $A=(7\pm1)\times10^{-21}$J is plotted against the experimental results (dashed lines for both figures). For silica D_{eq} =34±3Å, which is slightly greater

than the equilibrium distance for mica (D_{eq}=30±3Å) due to the greater fluctuations in the more hydrated membrane and roughness of the underlying silica support. The magnitude of adhesion force between membranes immobilized on silica, A_{dh}, is in agreement with theoretical predictions and previous measurements of DPPC membranes supported on inner leaflets of DPPC[17]. The adhesion is comparable between the two salt concentrations at about 0.65mN/m. Third, membranes on silica appear slightly more compressible due to the softer/rougher underlying silica layer. Fourth, the physisorption of the inner DPPC leaflet to silica is weaker than to mica and can be quantified by the lower transfer ratios during Langmuir Blodgett deposition.

In particular, the presence of an unexpected electrostatic interaction when membranes are supported on silica and presence of holes in the membrane could be important in biophysical membrane studies on glass and biosensor applications where selective binding of ligands or proteins to membranes is important.

Acknowledgments

This work was supported by NSF Chemistry Division through grant CHE-0957868 and from the NIH Training Grant in Biomolecular Technology awarded by the Designated Emphasis in Biotechnology at UC Davis. We also thank Daniel Kienle and Dennis Mulder for assistance with MMM modeling, William Chan for fluorescent microscopy measurements, and Gwen Schuman for her contributions in transfer ratio measurements.

References

1. Sackmann, E., Supported Membranes: Scientific and Practical Applications. *Science* **1996,** 271, (5245), 43-48

2. Leckband, D. I., J., Intermolecular Forces in Biology. *Quarterly Reviews of Biophysics* **2001,** 34, (2), **105–267**.

3. Claesson, P. E., T; Bergeron, V; et al., Techniques for measuring surface forces. *ADVANCES IN COLLOID AND INTERFACE SCIENCE* **1996,** 67, 119-183

4. Rand, R. P. P., V.A. , Hydration forces between phospholipid bilayers. *Biochim. Biophys. Acta* **1989,** 988 (3), 351-376.

5. Safinya, C. R.; Roux, D.; Smith, G. S.; Sinha, S. K.; Dimon, P.; Clark, N. A.; Bellocq, A. M., Steric Interactions in a Model Multimembrane System: A Synchrotron X-Ray Study. *Phys. Rev. Lett.* **1986**, 2718–2721.

6. Parsegian, V. A.; Fuller, N.; Rand, R. P., The role of long range forces in ordered arrays of tobacco mosaic virus. *Nature* **1979,** 259, 632±635.

7. Caffrey, M. B.; Bilderback, D. H., Realtime X-ray diffraction using synchrotron radiation: system characterization and applications. *Nucl. Instrum. Meth.* **1983,** 208, (495-510).

8. Nagle, J. T.-N., S, Structure of lipid bilayers *BIOCHIMICA ET BIOPHYSICA ACTA-REVIEWS ON BIOMEMBRANES* **2000,** 1469 (3), 159-195.

9. Petrache, H. G., N; Tristram-Nagle, S; et al., Interbilayer interactions from high-resolution x-ray scattering. *PHYSICAL REVIEW E* **1998,** 57, (6), 7014-7024

10. Evans, E. K., DJ; Rawicz, W; et al., Interactions between polymer-grafted membranes in concentrated solutions of free polymer. *LANGMUIR* **1996,** 12, (12), 3031-3037.

11. Evans, E. N., D. , Physical Properties of Surfactant Bilayer-Membranes - Thermal Transitions, Elasticity, Rigidity, Cohesion, and Colloidal Interactions. *JOURNAL OF PHYSICAL CHEMISTRY* **1987,** 91, (16), 4219-4228.

12. Evans, E. R., K; Merkel, R. , Sensitive Force Technique To Probe Molecular Adhesion and Structural Linkages at Biological Interfaces. *BIOPHYSICAL JOURNAL* **1995,** 68, (6), 2580-2587

13. Alessandrini, A. F., P., AFM: a versatile tool in biophysics *MEASUREMENT SCIENCE & TECHNOLOGY* **2005,** 16, (6), R65-R92

14. Garcia-Manyes, S.; Sanz, F., Nanomechanics of lipid bilayers by force spectroscopy with AFM: A perspective. *Biochimica et Biophysica Acta* **2010**, 741–749.

15. Pera, I.; Stark, R.; Kappl, M.; Butt, H.-J.; Benfenati, F., Using the Atomic Force Microscope to Study the Interaction between Two Solid Supported Lipid Bilayers and the Influence of Synapsin I. *Biophysical Journal* **2004,** 87, (4), 2446–2455.

16. Richter, R. P.; Brisson, A., Characterization of lipid bilayers and protein assemblies supported on rough surfaces by atomic force microscopy. *Langmuir* **2003,** 19 1632–1640

17. Marra, J., and Israelachvili, J., Direct Measurements of Forces between Phosphatidylcholine and Phosphatidylethanolamine Bilayers in Aqueous Electrolyte Solutions. *Biochemistry* **1985,** 24, 4608-4618.

18. Orozco-Alcaraz, R. K., T.L. , Impact of membrane Fluidity on Steric Stabilization by Lipopolymers. *Langmuir* **2012,** 28, 7470-7475.

19. Moore, N. W., and Kuhl, T. L., Bimodal Polymer Mushrooms: Compressive Forces and Specificity toward Receptor Surfaces. *Langmuir* **2006,** 22, 8485-8491.

20. Helm, C. A.; Israelachvili, J. N.; McGuiggan, P. M., ROLE OF HYDROPHOBIC FORCES IN BILAYER ADHESION AND FUSION. *Biochemistry* **1992,** 31, (6), 1794-1805.

21. Leckband, D. E., Helm, C.A., Israelachvili, J., Role of calcium in the adhesion and fusion of bilayers. *Biochemistry* **1993,** 32, (4), 1127-1140.

22. Sheth, S. R., Leckband, D., Measurements of attractive forces between proteins and end-grafted poly(ethylene glycol) chains. *Proceedings of the National Academy of Sciences of the United States of America* **1997,** 94, (16), 8399-8404.

23. Anderson, T. H. M., Y.; Weirich, K.L.; Zeng, H.; Fygenson, D.; Israelachvili, J.N., Formation of Supported Bilayers on Silica Substrates. *American Chemical Society* **2009,** 25, (12), 6997–7005.

24. Sackmann, E., Supported Membranes: Scientific and Practical Applications. *Science* **1996,** 271, (5245), 43-48.

25. Tamm, L. K. M., H. M., Supported phospholipid bilayers. *Biophys J.* **1985,** 47, 105-113.

26. Siegel, D. P., Inverted micellar intermediates and the transitions between lamellar, cubic, and inverted hexagonal lipid phases. II. Implications for membrane-membraneinteractions and membrane fusion. *Biophysical Journal* **1986,** 49, (6), 1171–1183.

27. Paulsson, M., Basement Membrane Proteins: Structure, Assembly, and Cellular Interactions. *Critical Reviews in Biochemistry and Molecular Biology* **1992,** 27, (1-2), 93-127.

28. Lorenza, B. K., R.; Sunnicka, E.; Geila, B.; Janshoff, A., Colloidal probe microscopy of membrane–membraneinteractions: From ligand–receptor recognition to fusion events. *Biophysical Chemistry* **2010,** 150, (1-3), 54–63.

29. Tanaka, M. S., E., Polymer-Supported membranes as models of the cell surface. *Nature* **2005,** 437, (29), 656-663.

30. Knoll, W.; Bender, K.; Förch, R.; Frank, C.; Götz, H.; Heibel, C.; Jenkins, T.; Jonas, U.; Kibrom, A.; Kügler, R., Polymer-Tethered Bimolecular Lipid Membranes. *Polymer Membranes/Biomembranes* **2010,** 224, 87-111.

31. Spinke, J.; Yang, J.; Wolf, H.; Liley, M.; Ringsdorf, H.; Knoll, W., Polymer-supported bilayer on a solid substrate. . *Biophysical Journal* **1992,** 63, (6), 1667.

32. Chi, L.; Anders, M.; Fuchs, H.; Johnston, R.; Ringsdorf, H., Domain structures in Langmuir-Blodgett films investigated by atomic force microscopy. *Science* **1993,** 259, (5092), 213.

33. Majewski, J. W., J.; Park, C.; Seitz, M.; Israelachvili, J.; Smith, G. , Structural studies of polymer-cushioned lipid bilayers. . *Biophysical Journal* **1998,** 75, (5), 2363-2367.

34. Wong, J. Y. M., J.; Seitz, M.; Park, C. K.; Israelachvili, J. N.; Smith, G. S. , Polymer-cushioned bilayers. I. A structural study of various preparation methods using neutron reflectometry. . *Biophysical Journal* **1999,** 77, (3), 1445-1457.

35. Baumgart, T. O., A. , Polysaccharide-supported planar bilayer lipid model membranes. . *Langmuir* **2003,** 19, (5), 1730-1737.

36. Wang, L. S., M.; Möhwald, H., Lipids coupled to polyelectrolyte multilayers: ultraslow diffusion and the dynamics of electrostatic interactions. . *The Journal of Physical Chemistry B* **2002,** 106, (35), 9135-9142.

37. Smith, H. L. J., M. S.; Vidyasagar, A.; Saiz, J.; Watkins, E.; Toomey, R.; Hurd, A. J.; Majewski, J., Model lipid membranes on a tunable polymer cushion. . *Physical Review Letters* **2009,** 102, (22), 228102.

38. Wagner, M. L. T., L. K., Tethered polymer-supported planar lipid bilayers for reconstitution of integral membrane proteins: silane-polyethyleneglycol-lipid as a cushion and covalent linker. . *Biophysical Journal* **2000,** 79, (3), 1400-1414.

39. Naumann, C. A. P., O.; Lehmann, T.; Rühe, J.; Knoll, W.; Frank, C. W., The polymer-supported phospholipid bilayer: tethering as a new approach to substrate-membrane stabilization. *Biomacromolecules* **2002,** 3, (1), 27-35.

40. Sinner, E. K. K., W. , Functional tethered membranes. . *Current opinion in chemical biology* **2001,** 5, (6), 705-711.

41. El-khouri, R. J. B., D.A.; Watkins, E.B.; Kim, C.Y.; Miller, C.E.; Patten, T.E.; Parikh, A.N.; Kuhl, T.L., pH Responsive Polymer Cushions for Probing Membrane Environment Interactions. *Nanoletters* **2011,** 11, (5), 2169–2172.

42. Vigil, G. X., Z.; Steinberg, S.; Israelachvili, J., Interactions of Silica Surfaces. *Colloid and Interface Science* **1994,** 165, 367-385.

43. Kuhl, T. L., Leckband, D. E., Lasic, D. D., and Israelachvili, J. N., Modulation of Interaction Forces Between Bilayers Exposing Short-Chained Ethylene Oxide Headgroups. *Biophysical Journal* **1994,** 66, 1479-1487

44. Kuhl, T. L., Leckband, D. E., Lasic, D. D., and Israelachvili, J. N., Modulation and Modeling of Interaction Forces Between Lipid Bilayers Exposing Terminally Grafted Polymer Chains. In *Stealth Liposomes*, Lasic, D. a. M., Frank., Ed. CRC Press: 1995; pp 73-91.

45. Klopfer, K. J. V., T. K., Isotherms of Dipalmitoylphosphatidylcholine (DPPC) Monolayers: Features Revealed and Features Obscured. *JOURNAL OF COLLOID AND INTERFACE SCIENCE* **1996,** 182, 220–229.

46. Israelachvili, J. N., and Adams, G. E., Measurement of Forces between Two Mica Surfaces in Aqueous Electrolyte Solutions in the Range 0-100 nm. *Chem. Soc., Faraday Trans.* **1978,** 74, 975-1001.

47. Israelachvili, J., Thin film studies using multiple beam interferometry. *J. Colloid Interface Science* **1973,** 44, 259.

48. Moore, N. W., Mulder, Dennis J., and Kuhl, Tonya L., Adhesion from Tethered Ligand-Receptor Bonds with Microsecond Lifetimes. *Langmuir* **2008,** 24, 1212-1218.

49. Valle-Delgado, J. J.; Molina-Bolivar, J. A.; Galisteo-Gonzalez, F.; GGalvez-Ruiz, M. J.; Feiler, A., Hydration forces between silica surfaces: Experimental data and predictions from different theories *Journal of Chemical Physics* **2005,** 123, (3).

50. Drelich, J., Long, J.; Xu, Z.; Masliyah, J.; White, C. L., Probing colloidal forces between a Si3N4 AFM tip and single nanoparticles of silica and alumina *Journal of Colloid and Interface Science* **2006,** 303, (2), 627-638.

51. Grabbe, A. H., R.G., Double-Layer and Hydration Forces Measured between Silica Sheets Subjected to Various Surface Treatments *Journal of Colloid and Interface Science* **1993,** 157, (2), 375-383

52. Scales, P. J. G., F.; Healy, T.W., Electrokinetics of the Silica-Solution Interface: A Flat Plate Streaming Potential Study. *Langmuir* **1992,** 8, (3), 965-974.

53. Schwer, C. K., E., Electrophoresis in Fused-Silica Capillaries: The Influence of Organic Solvents on the Electroosmotic Velocity and the Zeta Potential. *ANALYTICAL CHEMISTRY* **1991,** 63, (17), 1801-1807.

54. Valtiner, M.; Banquy, X.; Kristiansen, K.; Greene, G. W.; Israelachvili, J. N., The Electrochemical Surface Forces Apparatus: The Effect of Surface Roughness, Electrostatic Surface Potentials, and Anodic Oxide Growth on Interaction Forces, and Friction between Dissimilar Surfaces in Aqueous Solutions. *Langmuir* **2012,** 28, 13080−13093.

55. Valtiner, M.; Kristiansen, K.; Greene, G. W.; Israelachvili, J. N., Effect of Surface Roughness and Electrostatic Surface Potentials on Forces Between Dissimilar Surfaces in Aqueous Solution. *Advanced Materials* **2011,** 23, 2294–2299.

56. Axelrod, D.; Koppel, D. E.; Schlessinger, J.; Elson, E.; Webb, W. W., Mobility measurement by analysis of fluorescence photobleaching recovery kinetics. *Biophys. J.* **1976,** 16, 1055–1069.

57. Kloboucek, A.; Behrisch, A.; Faix, J.; Sackmann, E., Adhesion-Induced Receptor Segregation and Adhesion Plaque Formation: A Model Membrane Study. *Biophysical Journal* **1999,** 77, (4), 2311–2328.

58. Blonk, J. C.; Don, A.; Van Aalst, H.; Birmingham, J. J., Fluorescence photobleaching recovery in the confocal scanning light microscope. *J. Microscopy* **1992,** 169 363–374.

59. Castellana, E. T.; Cremer, P. S., Solid supported lipid bilayers: From biophysical studies to sensor design. *Surface Science Reports* **2006,** 61, 429–444.

60. Tanford, C., Micelle Shape and Size. *The Journal of Physical Chemistry* **1972,** 76, (21).

61. Small, D. M., Phase equilibria and structure of dry and hydrated egg lecithin. *Journal of Lipid Research* **1967,** 8, 551-557.

62. Kuhl, T. L., Berman, A.D., Hui, S.W., and Israelachvili, J. N. , Part 1. Direct Measurement of Depletion Attraction and Thin Film Viscosity between Lipid Bilayers in Aqueous Polyethylene Glycol Solutions. *Macromolecules* **1998,** 31, 8250-8257.

63. Pincet, F.; Cribier, S.; Perez, E., Bilayers of neutral lipids bear a small but significant charge. *European Physical Journal B* **1999,** 11, (1), 127-130.

64. Giasson, S. K., T.L.; Israelachvili, J.N., Adsorption and Interaction Forces of Micellar and Microemulsion Solutions in Ultrathin Films. *Langmuir* **1998,** 14, 891-898.

65. Nagle, J. F. W., M. C. , Structure of fully hydrated bilayer dispersions. *Biochim. Biophys. Acta* **1988,** 942, 1-10.

66. Watkins, E. B.; Miller, C. E.; Mulder, D. J.; Kuhl, T. L.; Majewski, J., Structure and orientational texture of self-organizing lipid bilayers *Phys. Rev. Lett.* **2009,** 102, (23).

67. Bassereau, P.; Pincet, F., Quantitative Analysis of Holes in Supported Bilayers Providing the Adsorption Energy of Surfactants on Solid Substrate. *Langmuir* **1997,** 13, 7003-7007.

68. Duncan, S. L.; Larson, R. G., Comparing Experimental and Simulated Pressure-Area Isotherms for DPPC. *Biophysics* **2008,** 94, (8), 2965–2986.

69. Ma, G.; Allen, H. C., DPPC Langmuir Monolayer at the Air-Water Interface: Probing the Tail and Head Groups by Vibrational Sum Frequency Generation Spectroscopy. *Langmuir* **2006,** 22, 5341-5349.

70. Van oss, C. J., Interfacial forces in Aqueous Media. In Marcel Dekker: New York, 1994.

71. Dufrene, Y. L., GU, Advances in the characterization of supported lipid films with the atomic force microscope. *Biochim. Biophys. Acta - Biomembranes* **2000,** 1509, (1-2), 14-41.

72. Hui, S. W. V., R.; Zasadzinski, J.A.; et al.,

The structure and stability of phospholipid-bilayers by atomic-force microscopy. *Biophys J.* **1995,** 68, (1), 171-178.

CHAPTER 3

Impact of membrane fluidity on steric stabilization by lipopolymers

Adapted with permission from Raquel Orozco-Alcaraz and Tonya L. Kuhl. Impact of membrane fluidity on steric stabilization by lipopolymers. *Langmuir*, **2012**, *28* (19), pp 7470–7475. 2012.

Abstract

In this work, the impact of lipid lateral mobility on the steric interaction between membranes containing polyethylene glycol (PEG) functionalized lipids was investigated using the Surface Force Apparatus. The force-distance profiles show the presence of electrostatic and steric repulsion that arise from the presence of negatively charged PEG functionalized lipids. Fluid phase bilayers have high lateral diffusion relative to gel phase bilayers; however a quantitative comparison of the interaction forces between membranes in these two different phase states demonstrates a reduced rate of diffusion in the fluid phase for the PEG-lipids under constrained geometries. This finding suggests that lateral friction between the opposing polymer chains is significant in restricted environments. As a result, binding affinity of ligated PEG chains used in liposomal drug delivery can only be modestly tailored by the phase state of the liposome.

Introduction

Because of its low toxicity, low protein absorption, non-ionic character, and solubility in both aqueous and organic solvents, polyethylene glycol (PEG) is the most commonly used polymer coating to biocompatibilize surfaces for biomedical applications[1-6]. One specific application involves the grafting of PEG to vesicle or liposome surfaces for drug delivery. By judicious choice of grafting density and PEG molecular weight, circulation half-lives of liposomes can be extended from hours to days due to reduced plasma interactions by the steric repulsive barrier presented by the

polymer chains[7-13]. As a result, PEG-coated liposomes have acquired the moniker "Stealth Liposomes™" due to their ability to evade the body's immune system. The enhanced circulation time allows Stealth Liposomes to accumulate inside tissues and tumors which leads to a drug-release system referred to as passive targeting[10].

However, extending circulation times is only part of the equation. It is also highly desirous to actively target the liposome to a specific diseased cell type, e.g. cancer cells. Towards this goal, there has been significant effort to functionalize PEG chains with specific ligands to provide selective targeting[10, 14-18]. In ex-vivo studies such as cell culture, selective targeting has been demonstrated to work with high efficiency[19]. Unfortunately, translating these bench top studies to animals or humans has not demonstrated significant benefit or increase in efficacy through targeting. While many studies of liposomal based technologies look promising, PEGylated liposomal doxorubicin (DOXIL/ Caelyx) has been the only approved liposomal formulation in the USA and Europe for Kaposi's sarcoma and recurrent ovarian cancer[20-22].

PEG steric stabilization clearly aids in circulation longevity, but it can also be viewed as a steric hindrance once the liposome reaches the active site[5]. It has been reported that reducing steric repulsion increases the net adhesive force of ligands to access receptor sites[16]. Though different formulations have been created to increase the binding effectiveness in targeting, it is important to understand the surface behavior of a PEGylated membrane when it comes to contact to another surface. Here, we investigate the impact of membrane fluidity and lateral mobility of PEG functionalized lipids on the steric interaction between two opposing membranes. In this system, the grafting density of the PEG chains in the contact region can dynamically respond to confinement and

diffuse along the lipid membrane surface. Consequently, fluidity can reduce steric hindrance once the liposomal surface reaches the target site. The measured reduction in the steric interaction is used to estimate the diffusion of the PEG functionalized lipids in the contact region between the opposing membranes.

Materials and Methods

Chemicals. 1,2-dipalmitoyl-*sn*-glycero-3-phosphoethanolamine (DPPE), 1,2-dimyristoyl-sn-glycero-3-phosphocholine (DMPC), 1,2-dimyristoyl-sn-glycero-3-phosphoethanolamine-N- [methoxy(polyethylene glycol)-2000] (ammonium salt) (DMPE-PEG2000), were purchased from Avanti Polar Lipids, Inc. (Alabaster, AL) and used as received.

Sample preparation. Supported lipid bilayers were prepared by Langmuir-Blodgett (LB) deposition using a temperature-controlled Wilhelmy Trough (Nima Coventry, UK) as described elsewhere[23-24]. Lipids were dissolved in 9:1 chloroform/methanol at a concentration of approximately 1 mg/ml. The bilayer surfaces were assembled onto molecularly-smooth, back-silvered mica substrates glued onto silica disks (Figure 1). A close-packed, solid phase inner monolayer of DPPE (~ 43 Å per molecule, Π= 40 mN/m) was first deposited by raising the substrates vertically through a compressed DPPE monolayer at the air-water interface yielding transfer ratios of 1.0 ± 0.05. Afterwards, an outer layer of 92.5 mole % DMPC + 7.5 mole % DMPE-PEG2000 was deposited onto the DPPE film at 35mN/m. The transfer ratios of the mixed outer monolayers were 0.99 ±0.03. DMPC was chosen as the matrix lipid because its phase transition temperature is

23.5°C [25], thus the temperature of the system can be easily manipulated to modify the diffusivity of the outer lipid layer; below 23.5°C in the solid phase D~0.02μm^2/sec [26] and above in the fluid phase D~4μm^2/sec [27].

Surface Force Measurements. The Surface Force Apparatus (SFA) was used to measure the interaction forces between the PEGylated bilayers. The SFA technique has been used extensively to measure interaction forces between surfaces[28-29]. The studies using this method provide a better understanding for inter-surface behavior between relatively large areas, compared to Atomic Force Microscopy (AFM) performed in previous studies[30]. After depositing the membranes on mica, the surfaces were transferred and mounted into the SFA under water, a procedure detailed elsewhere[31]. The water in the SFA box was saturated with a speckle of DMPC to prevent lipid desorption from the solid substrate. After the surfaces were mounted, the SFA box was placed in a temperature controlled room at 20°C, which is below DMPC's transition temperature. To measure the interacting forces when in the fluid phase, the temperature was later increased to 28°C. A custom automated SFA was used for convenient data collection[17]. The system enabled constant surface displacement via a computer controlled motor system. A sensitive CCD camera was interfaced with the spectrometer and computer acquisition system to allow automated wavelength determination of the fringes of equal chromatic order.

Bilayer-bilayer contact, D = 0, was defined as the contact between nominally dehydrated bilayers without any polymer layer[23]. Both PC and PE lipids are zwitterionic. However, PEG-functionalized lipids are negatively charged as the PEG chain is

covalently attached to the terminal amine head group of the DMPE lipid. Any electrostatic interaction between the membrane surfaces is therefore attributed to the presence of DMPE-PEG2000 (Figure 1). As the negative charge is at the phosphate group, the outer Helmholtz plane in the electrostatics analysis used the same reference of D = 0 as in the force profile measurements.

Results and Discussion

Isotherms for the various lipid monolayers: 100% DMPC, 100% DMPE-PEG2000, and 7.5 mol% DMPE-PEG2000 + 92.5 mol% DMPC, are shown in Figure 2**.** Lateral interactions between lipids and PEGylated lipids in monolayers at the air-water interface have been previously measured. It has been reported that above a critical pressure of ~10 mN/m, it is energetically more favorable for the polymer to extend into the water solution and that lipopolymer mixes with the lipid at the air-water interface [24, 32]. In this work with DMPC doped DMPE-PEG2000 monolayers, we observe the same phenomenon of PEG absorption to the air-water interface and then being squeezed into the water subphase with increasing lateral compression. To establish whether DMPC and DMPE-PEG2000 phase separate or mix, the isotherm of the monolayer doped with 7.5 mol% DMPE-PEG2000 was compared to that expected for ideal-mixed-behavior, expressed by equation 1:

$$A_x = xA_P + (1 - x)A_L \quad (1)$$

Here A_x is the average area of a molecule in mixture at the air-water interface, A_L is the area of a DMPC lipid in a pure monolayer, A_P is the area of a PEG2000 chain in a pure DMPE-PEG monolayer, and X is the mole fraction of DMPC in the mixed monolayer.

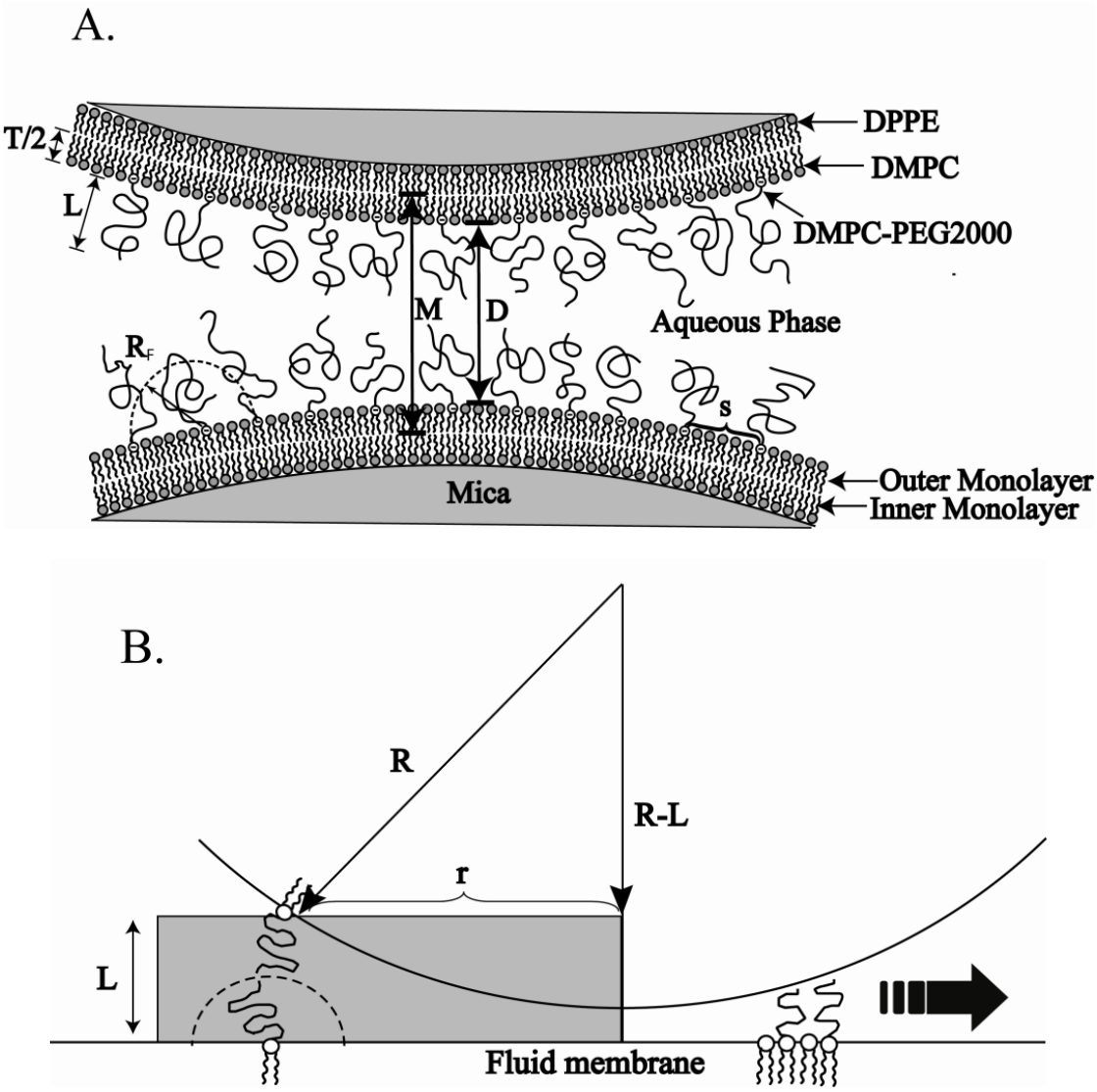

Figure 1. A) Illustration of the lipopolymer bilayer geometry in the SFA. RF denotes the Flory radius of the polymer chain, which is 35Å for PEG-200023-24. The average distance between PEG grafting sites is symbolized by s, where $\sigma = s^{-2}$ and σ is the lipopolymer-grafting density in the outer layer. M is the distance based on the contact between the inner DPPE monolayers, T/2 is the outer DMPC layer thickness, and L is the polymer layer thickness. D = 0 is defined as the contact between two "nominally" dehydrated bilayers, D = M-T. B) Illustration of maximum distance, r, a lipopolymer needs to travel in order to exit the contact zone between two surfaces. R is the radius of curvature of the cylindrical support surface.

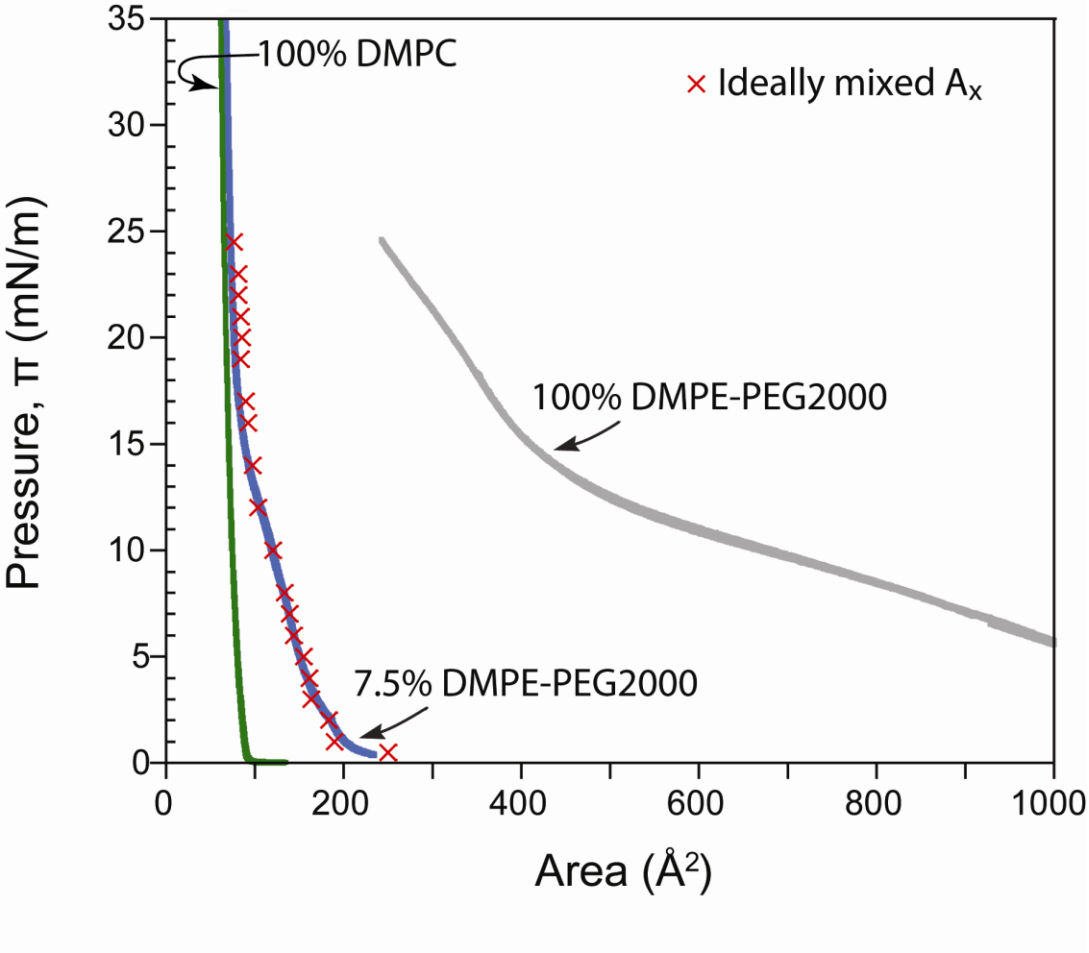

Figure 2. Surface pressure vs. area curve isotherms of: 100 mole% DMPC, 100 mole% DMPE-PEG2000, and 7.5mole% DMPE-PEG2000 + 92.5 mole% DMPC. Symbols (x) are the theoretical prediction if the mixture behaves ideally.

The x-points curve in Figure 2 displays A_x as a function of surface pressure, where A_L and A_P were obtained from the pure DMPC and DMPE-PEG2000 isotherms respectively. The A_x curve overlaps the isotherm obtained experimentally demonstrating that the system mixes ideally. As a result, the grafting density of the lipopolymer is readily obtainable from the mole % of lipopolymer and the area per lipid molecule. At 35mN/m, the average area per molecule is 57Å^2, a value consistent with previous measurements[33]. Thus, for the 92.5 mol % DMPC - 7.5 mole% DMPE-PEG monolayer, the area per grafted PEG chain, σ, is ~760Å^2 yielding a distance, *s*, of ~28Å between

grafting points. This concentration was selected to match to the grafting density of previously studied 4.5- 5 mole% DSPE-EO_{45} mixed in gel phase DSPE membranes[23-24]. Relative to the unperturbed polymer chain radius of gyration, $R_F = aN^{0.6} = 35$Å, this grafting density is in the overlapping mushroom regime, $\sigma^* = R_F^2/\sigma \approx 1.7$ [23-24, 34].

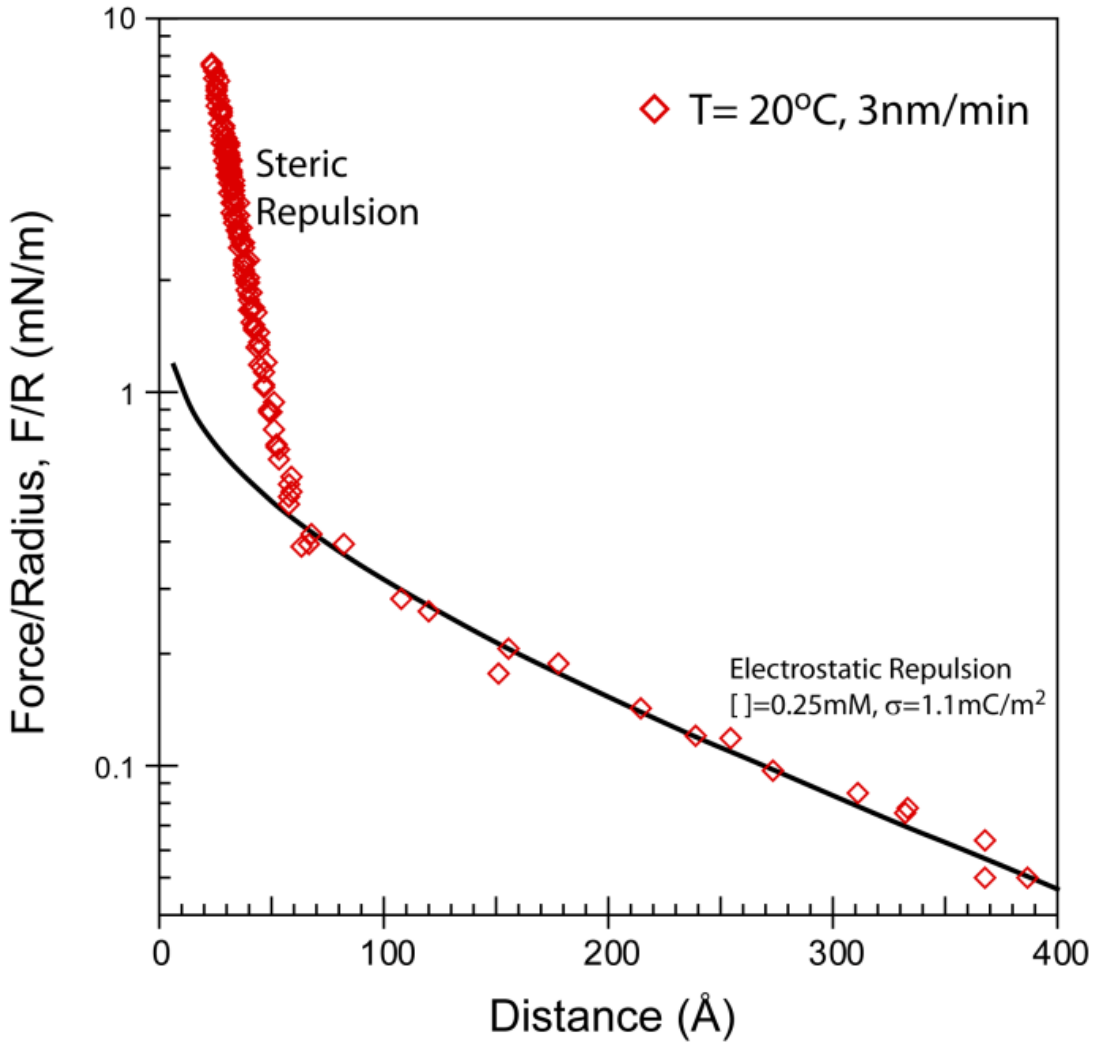

Figure 3. Force-distance profile of DMPC bilayers with a surface coverage of 7.5% DMPE-PEG2000 at 20°C. The electrostatic curve was fit using the concentration of $[NaNO_3]$ = 0.25mM and surface charge density of 1.1 mC/m^2.

Figure 3 shows an example force-distance profile between two DMPC bilayers doped with 7.5 mol% DMPE-PEG2000 at 20ºC. At this temperature the membrane is in the gel phase and the force profile matches results obtained with gel phase membranes containing 4.5 mol% DSPE-PEG2000[23-24]. As expected, the force-distance curve displays long range electrostatic and shorter range steric repulsion associated with the presence of the lipopolymers in the membranes. Theoretically and experimentally both the electrostatic and steric forces decay roughly exponentially. In the case of electrostatic forces, the decay is determined by the ionic strength (Debye length, κ^{-1}~200Å). In the weakly overlapping mushroom regime, the steric interaction has a characteristic decay length approximately the thickness of the polymer layer, $R_F = 35$Å, but for two layers would be $2R_F \approx 70$Å. Unless the two decay lengths are similar, a double-exponential curve is measured from which the electrostatic and steric contribution can be separated. The electrostatic contribution was determined by solving the nonlinear Poisson-Boltzmann equation explicitly using a numerical algorithm[35]. The solid line in Figure 3 is the electrostatic contribution of the force profile based on the parameters in Table 1 assuming the outer Helmholtz plane to reside at the lipid head group interface, identical to the reference frame for contact, D = 0**.** The electrostatic portion was then subtracted from the force profile and the remaining repulsive force was attributed to the steric repulsion due to the grafted polymer chains.

For comparison Figure 4 shows a series of steric force-distance profiles (after subtracting the electrostatic repulsion) obtained above and below the phase transition temperature of the membrane. Double-layer parameters for each of the experimental

conditions are summarized in Table 1. While diffusion is negligible when the membrane is in the solid phase (T<23.5ºC), this is not true when the membrane is in the fluid phase.

Temperature (°C)	Rate (nm/min)	Electrolyte [$NaNO_3$] (mM)	Debye Length κ^{-1}(Å)	Surface Charge Density, σ_e (mC/m^2)
20	3	0.25±0.02	195	1.10
28	4	0.25 ±0.02	200	1.25
28	0.1	0.25 ±0.02	200	1.30

Table 1. Double layer parameters used to subtract the long-range electrostatic contribution from all force measurements and summary of chain extension as function of rate of approach.

Indeed, as the surfaces approach each other, the increase in osmotic pressure provides a directed driving force for the lipopolymer to diffuse out of the contact zone. As a result, the measured electrostatic and steric repulsion when the membrane is in the fluid state will be dependent on the rate of approach and the amount of lipopolymer, if any, that remains between the membranes.

As shown in Figure 4, membrane fluidity clearly results in a decrease in measured repulsion between the membranes, indicating that the amount of lipopolymers present in the contact zone decreased. Both the onset of the repulsion and the magnitude decrease when the membranes are in the fluid phase. A simple back of the envelope calculation can be used to estimate the time for a lipopolymer to diffuse out of the contact zone from $\langle d^2 \rangle = 4\mathcal{D} \cdot time_{exp}$. As illustrated in Figure 1B the curvature of the contact zone (here ~1cm) and the polymer layer thickness, yields an effective distance of ~15μm. Using the measured diffusion of PEG-lipids in single supported membranes, D~4μm^2/sec, from Albertorio et al.[27], the expected time for the lipopolymer to diffuse out of the contact region is only $time_{exp} \cong$ 1min. Thus, an approach rate of 4nm/min is

sufficient for the lipopolymer to escape from the contact region. Even at a very slow approach rate of 0.1nm/min, which affords an order of magnitude increase in $time_{exp}$, lipopolymer clearly remains trapped between the approach surfaces – indicative of hindered diffusion. Kaufmann and coworkers[30] have determined that the mobility of PEG-lipids is reduced for concentrations above 6 mole % due likely to steric interactions of the polymer chains.

One approach to quantify the amount of polymer remaining between the membrane surfaces is to use polymer theory to model the resulting steric repulsion and extract the amount of PEGylated lipid from the theoretical fit to the data. Previous work has shown that the Alexander de Gennes (AdG) theory[36-38] and the self-consistent mean field theory of Milner, Witten, and Cates (MWC) both give a reasonable estimate for the compressive forces of grafted polymer brushes, even for systems that are not in the strongly stretched brush regime[24, 39]. In this case, we choose to use the MWC model as an explicit fit to the data without fitting parameters can be obtained. Assuming that the brushes have a parabolic profile and do not interdigitate, the force (F) normalized by the curvature of the cylindrical surfaces (R) as a function of separation distance (D), as measured in the SFA, $\frac{F}{R}$, can be obtained from MWC theory for the interaction energy between flat interfaces, E , using:

$$\frac{F}{R} = 2\pi(E(D) - E(h_o)) = \frac{2\pi h_o kT}{a^3}(a^2\sigma)^{\frac{4}{3}}\left(\frac{w}{a^3}\right)^{\frac{1}{3}}(a^2\nu)^{\frac{2}{3}}\left[\left(\frac{2h_o}{D}\right) + \left(\frac{D}{2h_o}\right)^2 - \left(\frac{D}{2h_o}\right)^5 - \frac{9}{5}\right] \quad (2)$$

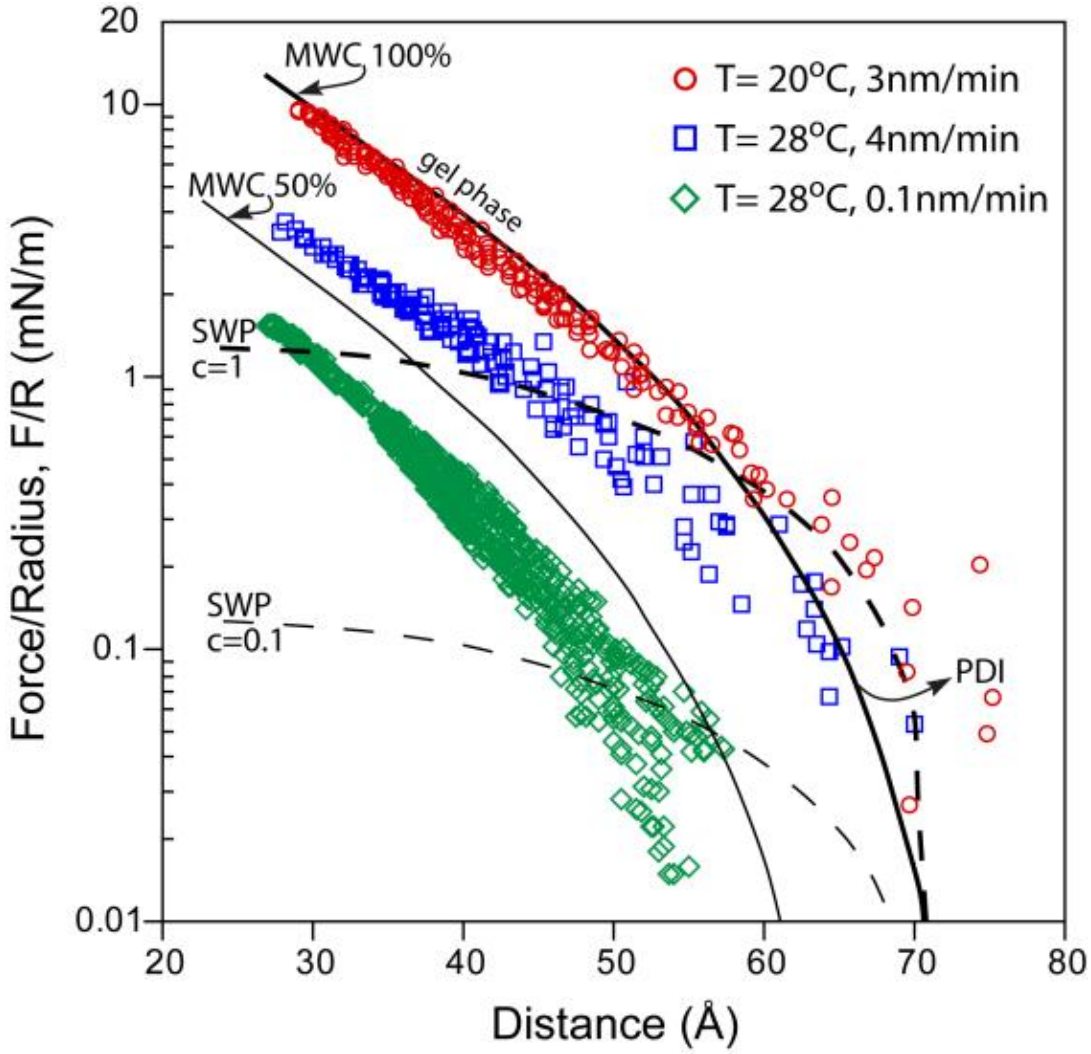

Figure 4. Steric Force-distance profiles between bilayers containing 7.5 mol% DMPE-PEG2000 as a function of approach rate. The steric forces were obtained by subtracting the electrostatic double-layer contribution. Approach rate: 3 nm/min at 20°C (○), 4nm/min at 28°C (□), 0.1nm/min at a 28°C (◇). The solid curves are fits to the MWC model (Equation 2). Solid heavy line indicates MWC fit in the gel-phase case. Thin solid curve represents the MWC model for 1/2 the initial grafting density. The dashed lines are predictions for the SWP model for surfaces bearing mobile polymer chains.

Where a (=3.5Å) is the size of a monomer, σ is the area per grafted chain, w is the excluded volume parameter ǂ, ν can be found from $R_F^2 = 3N/\nu$ or the statistical segment length, and the equilibrium extension of the polymer layer, ho, is given by:

$$h_0 = \left(\frac{12}{\pi^2}\right)^{\frac{1}{3}} N \cdot a \cdot (a^2\sigma)^{\frac{1}{3}} \left(\frac{w}{a^3}\right)^{\frac{1}{3}} (a^2\nu)^{-\frac{1}{3}} \quad (3)$$

For gel-phase membranes, σ was fixed to the known value of 1chain/760Å^2, w = (3.5Å)^3, and h_0 = 38Å. As shown in Figure 4, MWC provides an excellent fit to the data for D < 60Å. For small compressions (D > 60Å), the polydispersity (PDI~1.07) of the chains would have to be accounted for to accurately fit the data[40-41]. However, the MWC model is unable to properly account for the fluid phase membrane force profile data as the amount of lipopolymer between the membranes changes as a function of separation distance. For comparison, the MWC prediction for a system with a grafting density of ½ of the initial concentration (1chain/1520Å^2 *vs.* 1chain/760Å^2) is shown in Figure 4 (thin solid curve).

A more accurate way to determine the amount of polymer present in the contact zone with fluid membranes is to integrate the area under the curve to obtain total pressure for the contact area. Assuming that the total pressure arises strictly from osmotic repulsion then Morse equation[42] can be used to relate pressure (Π) and concentration in a straight forward manner:

$$\Pi = iMRT \quad (4)$$

where i is the dimensionless van't Hoff factor, M is the molarity; R the gas constant; and, T is the temperature. As the polymer concentration in the contact zone is known for the

ǂThe excluded volume parameter can be found from the osmotic pressure, Π, and volume fraction of PEG monomer in the brush via $\Pi = \frac{1}{2} w\phi^2 kT$. At an osmolality $c = 55\, moles/Kg$, the osmotic pressure is ~0.21MPa, yielding w = (3.48Å)$^3 \cong a^3$.

gel-phase case, the ratio of final lipopolymer concentration M_f, over initial concentration, M_0, can be interpreted as the % lipopolymer remaining at the contact zone, and can easily be obtained from the ratio of the integrated fluid to gel force profiles shown in Figure 4. Table 2 shows that the amount of polymer present in the contact zone decreases as the rate of approach decreases. Indeed at the slowest approach, 87% of the lipopolymer has escaped from the contacting region of the surfaces. A quantitative determination of the diffusion coefficient in this restricted geometry (Figure 1) would require development of the appropriate governing equation based on an osmotic pressure driving force. However, the effective diffusivity can simply be approximated from the contact geometry and measurement time at the slowest approach yielding $\mathcal{D} < 0.03 \frac{\mu m^2}{sec}$.

Rate (nm/min)	% Polymer remaining at the contact zone	Elapsed time (min)
3	100	N/A
4	45±5	1.5 ± 0.5
0.1	13±3	30 ± 3

Table 2. Estimation of % polymer remaining at the contact zone. Elapsed time starts when steric repulsion arising from the polymer layer is detected upon approach and ends when surface separation is initiated.

In regards to quantifying the experimentally measured steric force, Subramanian, Williams, and Pincus (SWP) provide an estimate of the total free energy when a surface bearing grafted but mobile polymer chains in the mushroom regime is compressed by a bare disc of area A_1 [43-44]. In their scaling model, the total free energy consists of two components; the energy to compress the mushrooms and translational entropic terms that account for the change in the initially, uniform grafting density, $\sigma = \sigma_0$, as chains leave

the region under the disc, $\sigma \rightarrow \sigma_1$, and move into the surrounding membrane, $\sigma \rightarrow \sigma_2$. Assuming the system is always at equilibrium and in the limit of low grafting density, $\sigma_0 R_F^2 << 1$, the free energy is minimized with respect to the density of chains under the disc, σ_1, and one finds:

$$E = c\sigma_0 kTA_1 \left[e^{-\left(L/D\right)^{\frac{5}{3}}} \right] \quad (5)$$

where L is the equilibrium, uncompressed extension of the chains, and c is a numerical prefactor. Accounting for the geometry of the SFA and that both surfaces have grafted chains yields:

$$\frac{F}{R} = 2\pi c\sigma_0 kT \left[e^{-1} - e^{-\left(2L/D\right)^{\frac{5}{3}}} \right] \quad (6)$$

The SWP model with c=0.1 and 1, is shown in Figure 4. Although the SWP model assumes an isolated mushroom steric contribution to the total energy, which is not appropriate for the conditions used in this work, some general comparisons can be made. First, in the model the repulsion raises rapidly as some compression of the layer is required to drive the chains from the confined region and overcome the pressure forcing mushrooms back under the disk. However, this "ideal gas" pressure is apparently below the experimental resolution, as no detectable steric force is observed at the slowest compression rate until D<60Å with is significantly less than the measured extension of the brush, 2L~70Å. With further compression, the steric force rapidly rises due to confinement but plateaus as the osmotic pressure provides a sufficient driving force to push chains from the confinement region into the bulk (non-confined region). In the experiments, lipopolymers are clearly driven out of the contact zone for modest compressions. However, a critical compression and resulting plateau in the force is not

seen in the experiments – rather the force rises rapidly for separation distances below ~55Å. These observations suggest that the diffusion of chains out of the contact zone becomes limited as the surface separation approaches the grafted chain radius of gyration. Given the expected, rapid diffusivity of the lipopolymers (~4μm^2/min), the trapping of chains in the compression region during the slowest compression implies that equilibrium during the compression was not maintained in the experimental system. Unfortunately, slower compression rates become prohibitive due to potential experimental drift. Although more complicated expressions for the steric force, e.g. MWC, could be used in the SWP model and may more accurately represent the experimental system, the stringent requirement of equilibrium is difficult to achieve.

Conclusion

In closing, direct measurement of the steric repulsion between membranes with embedded lipopolymers demonstrate that the amount of lipopolymer in the contact region is modulated when the membranes are in the fluid phase. The steric repulsion between the membranes decreases as a function of the approach rate due to osmotic pressure driven diffusion. Although a sufficiently slow approach should allow all lipopolymers to be depleted from the contact zone, we find that the diffusivity is significantly retarded and it is unlikely that equilibrium is maintained during the compression. Still, these findings imply potential avenues to improve targeted drug delivery vehicles. First, the steric barrier afforded by the embedded lipopolymers is critical to maintain circulation times by preventing non-specific protein absorption. The steric barrier afforded by the embedded lipopolymers is still substantial even in fluid membrane systems. Second, at

contact with another surface, these lipopolymers can be driven out of the contact zone if the membrane is fluid and thereby reduce the repulsion between the surfaces. Thus, an ideal scenario for drug delivery applications would involve a small percentage of ligated long chain lipopolymers in a forest of un-ligated "steric" bumpers to provide adhesion to the target surface while maintaining a strong steric barrier. The total amount of lipopolymers and the approach rate determines the magnitude of steric repulsion, while the inclusion of ligated lipopolymers can ensure that the contact/adhesion between the surfaces is maintained. Subsequently, the adhesion between the surfaces could be further augmented by an under-layer of short, ligated chains buried in the longer chained steric forest. Such a tiered system could provide robust steric repulsion that is converted to robust adhesion as the steric barrier presenting lipopolymers are excluded from the contact zone. Experimental measurements probing such tiered structures are currently underway.

Acknowledgements

The authors thank Dennis Mulder and Paul Bulkley-Logston for providing support in automating the Surface Force Apparatus and to Shari Williams for assisting in Langmuir monolayer experiments. This work was performed at UC Davis with support from NSF DMR-0606564. R.O.A. was partially supported by a Designated Emphasis in Biotechnology Fellowship.

References

1. Knop, K., Hoogenboom, R., Fischer, D., and Schubert, U.S., Poly(ethylene glycol) in Drug Delivery: Pros and Cons as Well as Potential Alternatives. *Angewandte Chemie International Edition* **2010,** 49, (36), 6288–6308.

2. Wischerhoff, E., et al. , Controlled Cell Adhesion on PEG-Based Switchable Surfaces. *Angewandte Chemie International Edition* **2008,** 47, (30), 5666–5668.

3. Jokerst, J. V., et al. , Nanoparticle PEGylation for imaging and therapy. *Nanomedicine* **2011,** 6, (4), 715-728.

4. Smet, M., Biological and Medical Applications of Hyperbranched Polymers. In *Hyperbranched Polymers: Synthesis, Properties, and Applications*, Deyue Yan, C. G., and Holger Frey, Ed. John Wiley & Sons, Inc.: Hoboken, NJ, USA, 2011; pp 387-412.

5. Ferrara, K., Pollard, R., Borden, M. , Ultrasound microbubble contrast agents: fundamentals and application to gene and drug delivery. *Annual Review of Biomedical Engineering* **2007,** 9, 415-47.

6. Lasic, D. D., Novel applications of liposomes. *Trends in Biotechnology* **1998,** 16, (7), 307-321

7. Wong, J., Kuhl, T., Israelachvili, J.N., Mullah, N., and Zalipsky, S., Direct measurement of a tethered ligand-receptor interaction potential *Science* **1997,** 275, (5301), 820-822.

8. Kenworthy, A. K., Simon, S.A., and McIntosh, T.J., Structure and phase behaviour of lipid suspensions containing phospholipids with covalently attached poly(ethylene glycol). *Biophysical Journal* **1995,** 68, (5), 1903-1920.

9. Lee, C.-M., et al., Polyethylene Glycol (PEG) Modified 99mTc-HMPAO Liposome for Improving Blood Circulation and Biodistribution: The Effect of the Extent of PEGylation. *Cancer Biotherapy & Radiopharmaceuticals* **2005,** 20, 620-628.

10. Immordino, M. L., Dosio, F., and Cattel, L., Stealth liposomes: review of the basic science, rationale, and clinical applications, existing and potential. *International Journal of Nanomedicine* **2006,** 1, (3), 297–315.

11. Vert, M., and Domurado D., Poly(ethylene glycol): protein-repulsive or albumin-compatible? *J Biomater Sci Polym Ed* **2000,** 11, 1307–17.

12. Kenworthy, A. K., Hristova, K., Needham, D., and McIntosh, T.J., Range and magnitude of the steric pressure between bilayers containing phospholipids with covalently attached poly(ethylene glycol). *Biophysical Journal* **1995,** 68, (5), 1921-1936.

13. Efremova, N. V., Huang, Y., Peppas, N.A., and Leckband, D.E., Direct measurements of interactions between thethered poly(ethylene glycol) chains and adsorbed mucin layers. *Langmuir* **2002,** 18, (3), 836-845.

14. Evans, E., Leung, A., Hammer, D., and Simon, S., Chemically distinct transition states govenrn rapid dissociation of single L-selectin bonds under force. *PNAS* **2001,** 98, (7), 3784-3789.

15. Moore, W. N. a. K., T.L., The role od flexible tethers in multiple ligand-receptor bond formation between curved surfaces. *Biophysical Journal* **2006,** 91, (5), 1675-1687.

16. Moore, N. W., and Kuhl, T. L., Bimodal Polymer Mushrooms: Compressive Forces and Specificity toward Receptor Surfaces. *Langmuir* **2006,** 22, 8485-8491.

17. Moore, N. W., Mulder, Dennis J., and Kuhl, Tonya L., Adhesion from Tethered Ligand-Receptor Bonds with Microsecond Lifetimes. *Langmuir* **2008,** 24, 1212-1218.

18. Terada, T., Iwai, M., Kawakami, S., Yamashita, F., and Hashida, M., Novel PEG-matrix metalloproteinase-2 cleavable peptide-lipid containing galactosylated liposomes for hepatocellular carcinoma-selective targeting. *Controlled Release* **2006,** 111, 333–342.

19. Hussain, S., Pluckthun, A., Allen, T.M., and Zangemeister-Wittke, U., Chemosensitization of carcinoma cells using epithelial cell adhesion molecule–targeted liposomal antisense against bcl-2/bcl-xL. . *Molecular Cancer Therapeuthics* **2006,** 5, (11), 3170-3180.

20. Krown, S. E., Northfelt, D.W., Osoba, D., et al., Use of liposomal anthracyclines in Kaposi's sarcoma. *Semin Oncol* **2004,** 31, 36–52.

21. Rose, P. G., Pegylated liposomal doxorubicin: optimizing the dosing schedule in ovarian cancer. *Oncologist* **2005,** 10, 205–14.

22. Mufamadi, M. S., et al. , A Review on Composite Liposomal Technologies for Specialized Drug Delivery. *Journal of Drug Delivery* **2011,** 2011.

23. Kuhl, T. L., Leckband, D. E., Lasic, D. D., and Israelachvili, J. N., Modulation of Interaction Forces Between Bilayers Exposing Short-Chained Ethylene Oxide Headgroups. *Biophysical Journal* **1994,** 66, 1479-1487

24. Kuhl, T. L., Leckband, D. E., Lasic, D. D., and Israelachvili, J. N., Modulation and Modeling of Interaction Forces Between Lipid Bilayers Exposing Terminally Grafted Polymer Chains. In *Stealth Liposomes*, Lasic, D. a. M., Frank., Ed. CRC Press: 1995; pp 73-91.

25. Kaneshina, S., et al., Partitioning of local anesthetic dibucaine into bilayer membranes of dimyristoylphosphatidylcholine. *Colloids and Surfaces B: Biointerface* **1997,** 10, 51-57.

26. Tamm, L. K. a. M., H.M., Supported Phospholipid Bilayers. *Biophysical Journal* **1985,** 47.

27. Albertorio, F., Diaz, A.J., Yang, T., Chapa, V.A., Kataoka, S., Castellana, E.T., Cremer, P.S., Fluid and Air-Stable Lipopolymer Membranes for Biosensor Applications. *Langmuir* **2005,** 21, 7476-7482.

28. Israelachvili, J. N., and Adams, G. E., Measurement of Forces between Two Mica Surfaces in Aqueous Electrolyte Solutions in the Range 0-100 nm. *Chem. Soc., Faraday Trans.* **1978,** 74, 975-1001.

29. Israelachvili, J., Thin film studies using multiple beam interferometry. *J. Colloid Interface Science* **1973,** 44, 259.

30. Kaufmann, S., Borisov, O., Textor, M., and Reimhult, E., Mechanical Properties of mushroom and brush poly(ethylene glycol)-phospholipid membranes. *Soft Matter* **2011,** 7, 9267-9275.

31. Marra, J., and Israelachvili, J., Direct Measurements of Forces between Phosphatidylcholine and Phosphatidylethanolamine Bilayers in Aqueous Electrolyte Solutions. *Biochemistry* **1985,** 24, 4608-4618.

32. Kuzmenka, D. J., Granick, S, Collapse of poly(ethylene oxide) monolayers. *Macromolecules* **1988,** 21, (3), 779-782.

33. Ritchie, T. K., et al. , Chapter 11 - Reconstitution of membrane proteins in phospholipid bilayer nanodiscs. In *Mrthods in Enzymology*, Duzgunes, N., Ed. Elsevier Inc: 2009; Vol. 464, pp 211-231.

34. Szleifer, I., Statistical thermodynamics of polymers near surfaces. *Current opinion in colloid & interface science* **1996**, 416-423.

35. Grabbe, A. a. H., R.G., Double-Layer and Hydration Forces Measured between Silica Sheets Subjected to Various Surface Treatments *Journal of Colloid and Interface Science* **1993,** 157, (2), 375-383

36. Alexander, S., Adsorption of chain molecules with a polar head, a scaling desciption. *J. Phys (Paris)* **1977,** 38, 983.

37. de Gennes, P., Polymer solutions near an interface. I. Adsorption and depletion layers. *Macromolecules* **1981,** 14, 1637.

38. de Gennes, P., Polymers at an interface; a simplified view. *Adv. Colloid Interface Sci* **1987,** 27.

39. Efremova, N. V., Bondurant, B., O'Brien, D.F., and Leckband, D.E. , Measurements of interbilayer forces and protein adsorption on uncharged lipid bilayers displaying poly(ethylene glycol) chains. *Biochemistry* **2000,** 39, (12), 3441-3451.

40. Milner, S. T., Compressing Polymer "Brushes": a Quantitative Comparison of Theory and Experiment *Europhys. Lett.* **1988,** 7, (8), 695-699.

41. Alonzo, J. M., J.W., and Kilbey II, S.M Forces of interaction between surfaces bearing looped polymer brushes in good solvent *Soft Matter* **2009,** 5, 1897-1904.

42. Amiji, M. M., and Sandmann, B.J. , Physical Properties of Solutions. In *Applied Physical Pharmacy*, Brown, M., and Sheinis, L.A. , Ed. McGraw-Hill Companies, Inc.: New York, USA, 2002; pp 55-56.

43. Subramanian, G., Williams, D.R.M., and Pincus P.A. , Interaction between Finite-Sized Particles and End Grafted Polymers. *Macromolecules* **1996,** 29, 4045-4050.

44. Subramanian, G., Williams, D.R.M., and Pincus P.A., Escape Transitions and Force Laws for Compressed Polymer Mushrooms. *EUROPHYSICS LETTERS* **1995,** 29, (4), 285-290.

CHAPTER 4

Mechanical Properties of Endothelial Cells

Abstract

The young moduli for single endothelial cells were directly measured using the Surface Force Apparatus (SFA). We describe how bovine aorta endothelial cells (BAECs) were mounted in the SFA box and visualized before cell compression. Our goal is to understand the surface behavior of the cells, thus we limit the cell deformation to < 7% deformation. The Hertzian and Capsule Model were utilized to analyze the stress vs. deformation curves obtained experimentally. We report a young's modulus of 87-2800MPa if the Capsule Model is used and 93-902kPa if the Hertzian Model is used. The values for both models have been consistently different by three orders of magnitude, with the Capsule Model providing a better fit. Results indicate that endothelial cells have a higher Young modulus and bending modulus than macrophage cells and we describe possible reasons why this discrepancy exists.

Introduction

Endothelial cell membranes have active functional molecules on their surface, including proteoglycans, glycoproteins, and glycolipids. The detailed sequences of the carbohydrate and protein components of these molecules play a central role in the biological activity of the cell.[1] These glycomolecules lie on the luminal side of the endothelial cell surface and form a polyelectrolyte brush layer better known as the glycocalyx. The glycocalyx acts as a vascular permeability barrier, protects and lubricates the cell from mechanical and chemical damage, and inhibits coagulation as well as leukocyte and platelet adhesion.[2-3] The properties of the glycocalyx are also important for

several applications including improvement of liposome uptake for drug delivery and therapeutic targeting[1, 4], white cell rolling on the endothelium during an immune response[5], atherosclerosis studies[6], and mechanotransduction[3] among others.[7-8]

Our understanding of the glycocalyx's structural properties has mainly evolved from microscopy studies that mainly sought to determine the thickness of the glycocalyx. For example, Squire et al. carried out a series of electron microscopy studies where they determined that the thickness of the glycocalyx of endothelial cells, originated from frog mesentery capillaries[9], was approximately 50-100nm.[10] However, the fixation required for electron microscopy studies may damage or alter the structure of the extracellular matrix decreasing the reliability of such measurements. Later work by Damiano et al. used microparticle image velocimetry to infer the extent of the glycocalyx in vivo.[11-12] It was shown that the hydrodynamically relevant endothelial layer present *in vivo* (0.5mm) was greatly diminished for endothelial cells cultured under standard, static conditions *in vitro* (0.02-0.03mm). Fundamental mechanical properties of live endothelial cells, such as the force required for compression, behavior and response to compression, and Young's modulus are still unknown and such information is potentially helpful for improving therapeutic targeting and to expand our understanding of the fundamental structure-function and materials properties of the glycocalyx.[3, 6-7]

The Surface Force Apparatus (SFA) has been used extensively to measure the force, energy, or pressure vs. distance profiles between two surfaces with high precision.[13-14] In short, this apparatus enables measurement of the interaction force between two crossed cylindrical surfaces as a function of their absolute separation. One of the surfaces is mounted on a weak double cantilever spring (Figure 1A) providing a

force sensitivity of order 50pN. White-light interferometry is used to measure the absolute distance between the two surfaces with angstrom resolution. Knowing the spring constant and displacement between the surfaces allows for the force-distance measurements between the two surfaces. Importantly, the contact area between the surfaces is roughly the size of a single endothelial cell.

Using the SFA, the force to compress single, live BAECs was measured. In addition, the force measurements are converted to stress-strain curves to quantify the Young's modulus under low, intermediate, and high strain. Finally, we compare these results to other measurements of cell mechanical properties.

Experimental Methods

Cell Culture

Bovine aortic endothelial cells (BAECs) were obtained from Cell Systems (Kirkland, WA). BAECs were cultured under standard procedures described in CSC Complete Medium by Cell Systems. BAECs used in this study were between passages 3–9. Dulbecco's Phosphate Buffered Saline (PBS) was purchased from Sigma-Aldrich (St. Louis, MO, USA). Nano pure water used was obtained from Millipore Gradient A purification system with a resistivity of 18MΩcm.

Culture Media and PBS

Using aseptic techniques, BAECS were cultured in t-flasks with Dulbecco's Modified Eagle's Medium (DMEM)/F12, 10% Fetalplex serum, and 1% penicillin

streptomycin. Using standard culture techniques, cells were detached at confluence, suspended, and then seeded at very low concentration onto surfaces for SFA measurements (see Figure 1B). The disk with seeded cells was then placed in the incubator (37°C and 5%CO_2) to allow the cells time to attach to the surface.

To minimize light scatter during the SFA measurements, PBS buffer was used instead of full medium as it is optically transparent and suitable for enabling endothelial cell survival for several hours at physiological temperature. After the cells were seeded for a few hours in the incubator, the SFA surfaces were removed and rinsed with PBS several times to effectively replace the full medium for PBS. The cells were used for force measurements for less than two hours after removal from the incubator and immersion in PBS buffer to ensure their viability.

Substrates

The SFA method primarily employs molecularly smooth, muscovite mica substrates of a uniform thickness (3-4microns). Muscovite mica is chemically inert and widely used as a solid support for force spectroscopy and fluorescence microscopy measurements. Freshly cleaved mica sheets are coated with a 550Å layer of silver and a fixed silver side down to cylindrical silica support disks (radius = 1.5cm) for experimental measurements. Endothelial cells, which are cultured in monolayers, must attach to a substrate to grow and proliferate.[15-17] Because morphology and proliferation of cells depends on the substrate and culture conditions[18], we compared BAEC morphology and growth rate between mica and the t-flasks used for culturing. We observed little

difference between mica and t-flasks used for passaging and culturing, making mica a suitable substrate for the experiments.

Surface Force Apparatus (SFA)

As stated earlier an SFA was employed to measure the compressibility of the BAEC seeded cells on mica substrates. Figure 1A is a schematic of the SFA box and Figure 1B is a typical phase microscopy image of a cell selected for SFA measurements seen through the microscope objective. As mentioned previously, cells are seeded on mica supported on a silica disk of cylindrical geometry and the opposing mica supported silica disk is staged such that the opposing surfaces have a cross-cylindrical configuration (Figure 1A). The typical contact area of the crossed cylinders is 70-100 μm^2. Figure 1A also illustrates how white light enters the SFA box and passes normally though the optical interferometer created by the back silvered mica substrates. The resulting constructive light interference consists of discrete wavelengths $\lambda_n^0 (n = 1,2,3 \ldots)$ that are separated in a spectrometer as Fringes of Equal Chromatic Order (FECO). When the surfaces are separated, the wavelength, λ_n^D, increases by a distance D. At large separations (>10,000Å), an approximate solution to the optical interferometer can be used to determine the surface separation can be used[13]:

$$D = \frac{1}{(\lambda_{p-1} - \lambda_p)} \left[\frac{\lambda_p \lambda_{p-1}}{2\mu} + \lambda_{p-1} T_p - \lambda_p T_{p-1} \right] \quad (1)$$

Where λ_p and λ_{p-1} are adjacent fringes of unknown order p and situated between λ_n^0 and λ_{n-1}^D. T_{p-1} is the distance calculated assuming λ_{p-1} has shifted from λ_n^0. If $\lambda_p = \lambda_n^0$ then

T_p=0. μ is the refractive index of the liquid used. Contact, or D=0, in the reported data was based on mica-mica contact in the absence of cells. Equation 1 is derived from the analytical solution of a three layer interferometer.

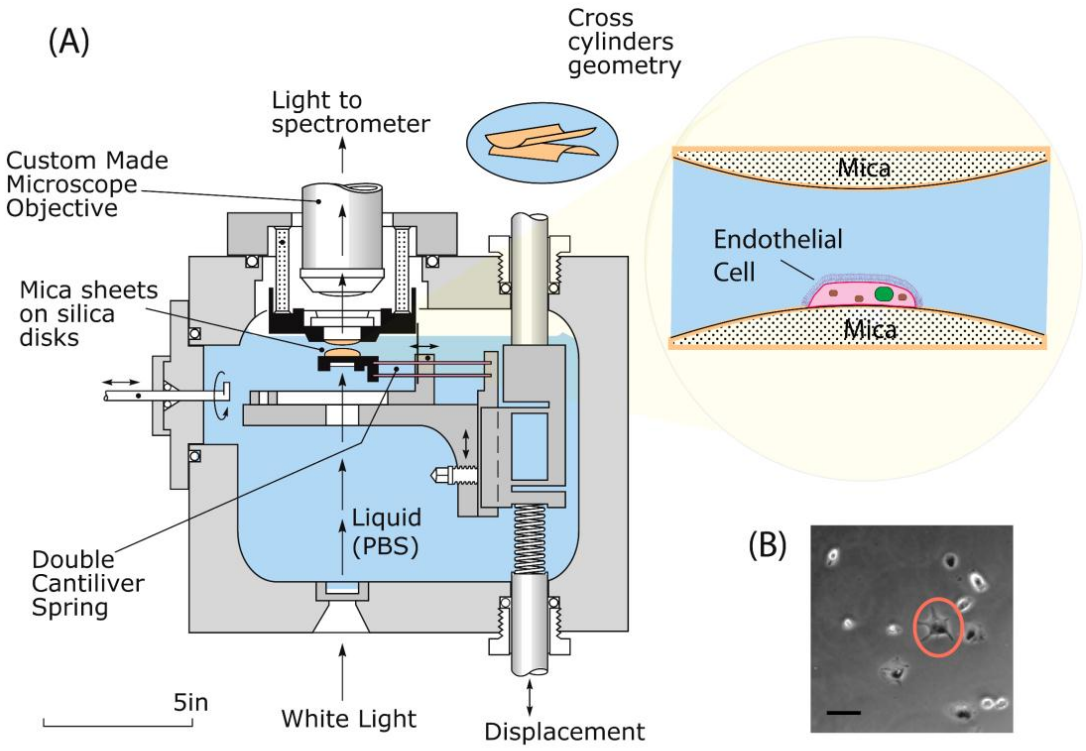

Figure 1. (A) Schematic of the surface force apparatus. (B) Micrograph of a typical BAEC cell selected for force runs. The horizontal line in the cell figure represents 25 μm

Results and Discussion

Force runs between single BAECs and a bare mica substrate were carried out in PBS using the SFA. Multiple measurements on different cells were performed and their force-distance profiles are shown in Figure 2.

The reference frame for the set of all curves is based on last compression point for each cell. It is presented in this format to show that the compression for single cells is not

necessarily reversible, hysteresis is present, and that cells, as expected, do not posses identical behavior. However, based on the single cell measurements performed (Figure 2), we were able to obtain an envelope of force-distance profiles that can provide a range of values that are unique for these types of cells. The inset in Figure 2 is the curve from the stiffest cell measured. The reference frame for this curve (D=0) is mica-mica and therefore it is possible to obtain the cell height from these profile. Overall the cell height for the measured cells (not included in Figure 2) was >2µm.

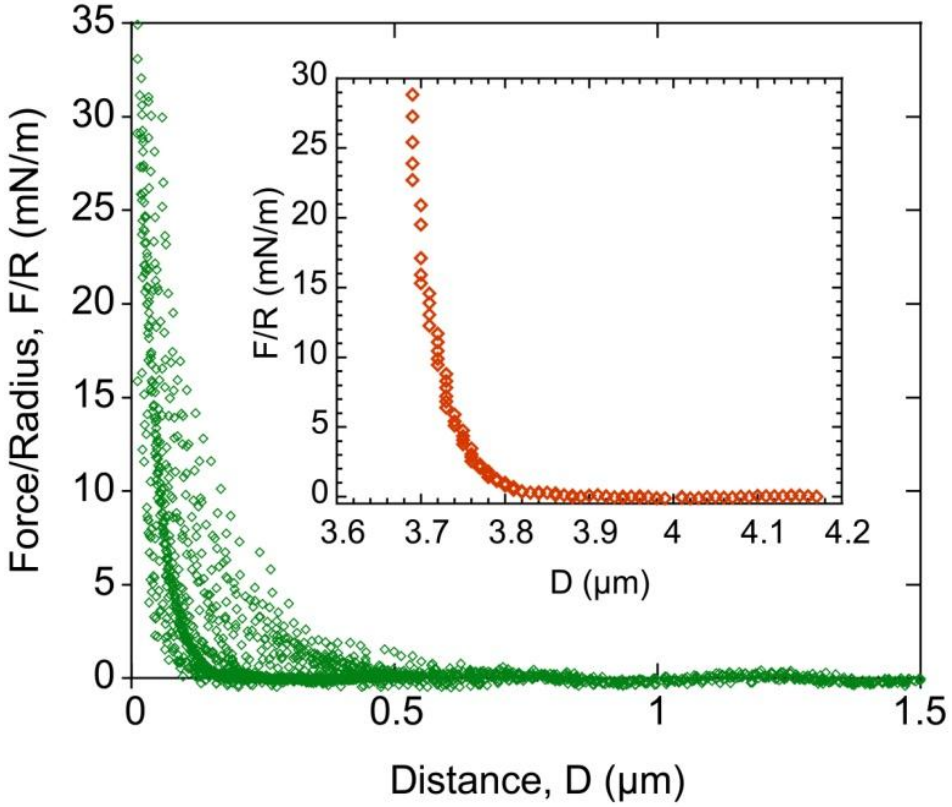

Figure 2. F_{exp}/R vs. Distance profiles for compression of multiple single BAECs. The reference frame is based on the last point of compression for each cell. Inset in this figure is a curve taken from set of profiles that form an envelope (in this case it's the curve that leads to a higher Young modulus). The reference frame for this curve (D=0) is mica-mica contact.

The SFA measures the force-distance (F-D) profile between two cross cylindrical surfaces. The force is usually normalized by the effective radius of curvature (R) of the opposing surfaces to account for differences in contact area. To extract mechanical properties, we followed the proposed method by Banquy et al.[19] where the experimental force, F_{exp}, is normalized by $2\pi RDN_D$.[19-20] Where D is the distance between surfaces (with mica-mica contact happening at D=0) and N_D is the cell density or $1cell/\pi R_c^2$ where R_c is the cell radius.

$$F(D) = F_{exp}/ (2\pi RDN_D) = F_{exp}\, R_c^2/2RD \quad (2)$$

Typically R_c is the radius of a spherical shaped cell and it is usually half of the cell height. Because endothelial cells are not necessarily spherical and usually have elongated morphology,[21] we cannot make this assumption. To obtain a general expression independent of the cell radius for force, we divided the above expression (Equation 2) by R_c^2:

$$F(D)/ R_c^2 = F_{exp} /2RD \quad (3)$$

Deformation is defined as $\delta = \left(1 - \frac{D}{L_0}\right)$ where L_0 is the initial height of the cell when deformation is zero. Figure 3 shows the normalized force profiles based on Equation 3 vs. deformation, δ, curves for the stiffest and the softest cell compression profiles measured.

The Hertzian Model (HM) was used fit to the data. HM has been used previously to model and extract mechanical properties of compressed spherical shaped cells such as macrophage and T lymphoma cells.[19, 22] This model is based on the contact theory of homogeneous elastic spheres. One of the assumptions implies cell incompressibility (only

elastic deformation) and that the cell membrane is impermeable. In addition, the model further assumes no adhesion or friction between the bodies at contact. The model relates the force, F, to compress two bodies to their Young's modulus, *E*:

$$F = \frac{\sqrt{2}E}{3(1-\nu_m{}^2)} R_c^2 \delta^{\frac{3}{2}} \quad (4)$$

Where ν_m is the Poisson ratio (ν_m=0.5 for an incompressible liquid inside an impermeable membrane), and R_c is the radius of contact area or in this case the radius of the cell.[23] As seen by the dotted curves in Figure 3, this model provides a satisfactory fit to the stiff cell experimental data over the full deformation range. The *E* values obtained from this model are summarized in Table 1.

Also employed to fit the experimental data was The Capsule Model, shown in Figure 3-dashed curves. This model describes the compressive behavior of a balloon filled with an incompressible fluid.[19, 24] In the past it has been utilized to model the compression of spherical shaped cells. Assuming impermeability and incompressibility of the fluid inside, the force contributions upon loading come from the stretching and bending of the cell membrane.

$$F = 2\pi \frac{E}{1-\upsilon_m} h R_c \delta^3 + \pi \frac{E}{2\sqrt{2}} h^2 \delta^{\frac{1}{2}} \quad (5)$$

The first term corresponds to the stretching force and the second term represents the bending force. Here *h* is the membrane thickness which is about 4nm for cell membranes. In a simple calculation, Lulevich et al.[24] showed that for small deformations, the bending force term of equation (5) can be neglected, leading to a simplified form of the Capsule Model:

$$F = 2\pi \frac{E}{1-\upsilon_m} hR_c\delta^3 \quad (6)$$

This simpler form provides a better fit (**Figure 3**) than the full form (not shown in our analysis).

In addition to the Young's modulus, the Capsule Model provides an expression for the bending modulus[19, 24-25], K :

$$K = \frac{Eh^3}{12(1-\nu_m{}^2)} \quad (7)$$

The values for the bending moduli are summarized in Table 1.

Table 1. Summary of elastic and bending moduli extracted from the stiffer and softer profiles measured

	Hertzian Model Elastic Modulus, E (kPa)	Simplified Capsule Model Elastic Modulus, E (MPa)	Bending Modulus, K, (kT)*
Stiffer Cell	321±19	479±14	828±24
Softer Cell	94±8	86±4	149±7

*T= 298K

Comparing our values with previous literature, we see that our values for the softer cell compression are within the same order of magnitude of the values reported in literature.[19, 24] Lulevich et al.[22] used the Capsule Model for live single cells but did not compare his reported values to the Hertzian Model. Instead, the Hertzian model was used to fit dead and fixed dead cells only. This previous work showed that using the Capsule Model, the Young modulus for the compression of single live T-cells is 10-30MPa and cells burst at a deformation of about 30%.[24] Our work was focused on measuring the cell surface deformation and thus did not surpass a deformation of 7% in order to preserve the

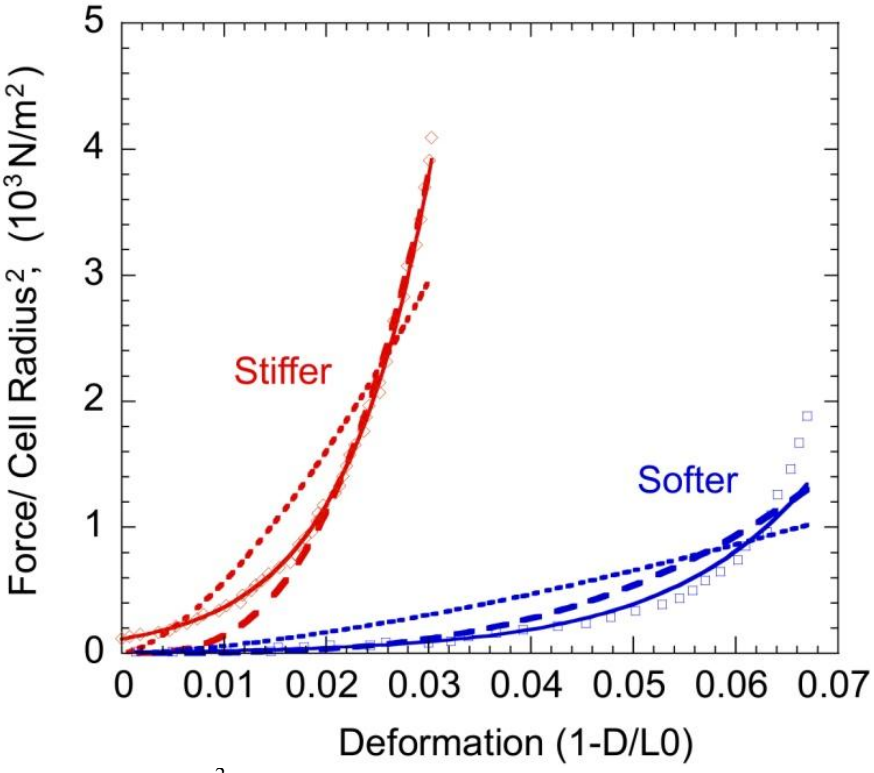

Figure 3. Force/Cell Radius^2 vs. Deformation curves for single endothelial cells. The experimental curves display the stiffer (diamond) and the softer (squares) profiles measured in our experiments. The solid curves are an exponential fit to the experimental data. Fits to the Hertzian Model are shown in dotted curves. The dashed curves are fits to the Simplified Capsule Model (assume stretching deformation only)

cell viability. We report values that are based on the stiffest and the softest case scenario after measuring multiple cells. Looking at our values, we see that the *E* values for the Hertzian Model are three orders of magnitude smaller than the values obtained for the Capsule Model. Other studies by Banquy et al.[19] have measured the compression of macrophage monolayer using the SFA and report an *E*=2-6.5MPa using the Capsule Model and 10-35kPa using the Hertzian model. Interestingly, this previous work demonstrates that their values from both models have a consistent three order of magnitude difference. It was suggested that the Hertzian Model[19] does not provide a good estimate for deformations greater than 30%. In our experiments, however, we did

not surpass a deformation greater than 7%. These results suggest that endothelial cells are stiffer than macrophages and T-lymphoma cells. This makes sense as the other type of cells can easily change conformation while endothelial cells are less mobile and deformable.

Conclusion

We demonstrated a detailed method of how to mount single BAEC cells in the SFA and showed that sensitive enough to measure the compressibility of single endothelial cells and established. Unlike other studies, we demonstrate that cells do not have a uniform behavior. The mechanical properties of single endothelial cells were quantified and compared to the elasticity macrophages and T-lymphoma cells. We established that BAECS are relatively stiffer, which makes sense as they are cells that have limited deformability compared to macrophages.

References

1. Baldeschwieler, J. D.; Schmidt, P. G., Liposomal drugs: from setbacks to success. *American Chemical Society* **1997,** 27, (10), 34-42.

2. Nieuwdorp, M. e. a., The endothelial glycocalyx: a potential barrier between health and vascular disease. *Current Opinion in Lipidology* **2005,** 16, 507-511.

3. Weinbaum, S.; al., e., Mechanotransduction and flow across the endothelial glycocalyx. *PNAS* **2003,** 100, (13), 7988–7995.

4. Lestini, B. L.; al., e., Surface modification of liposomes for selective cell targeting in cardiovascular drug delivery. *Journal of Controlled Release* **2002,** 78, 235–247.

5. Zhao, Y.; Chien, S.; Weinbaum, S., Dynamic contact forces on leukocyte microvilli and their penetration of the endothelial glycocalyx. *Biophys. Journal* **2001,** 80, 1124–1140.

6. Gouverneu, M.; Van der Berg, V.; Nieuwdorp, M.; Stroes, E.; Vink, H., Vasculoprotective properties of the endothelial glycocalyx: effects of fluid shear stress. *Journal of Internal Medicine* **2006,** 259, 393-400.

7. Damiano, E. R., The effect of the endothelial-cell glycocalyx on the motion of red blood cells through capillaries. *Microvasc. Res.* **1998,** 55, 77–91.

8. Weinbaum, S., 1997 Whitaker Distinguished Lecture: Models to Solve Mysteries in Biomechanics at the Cellular Level; A New View of Fiber Matrix Layers. *Annals of Biomedical Engineering* **1998,** 26 627–643.

9. Luther, P. K.; Michel, C. C.; Ryan, U. S.; Squire, J. M., Investigation of the surfaces of cultured endothelial cells for regular arrays of molecules using diffraction analysis of electron micrographs. *J. Physiol.* **1989,** 413, 2P.

10. Squire, J. M.; Chew, M.; Nneji, G.; Neal, C.; Barry, J.; Michel, C., Quasi-Periodic Substructure in the Microvessel Endothelial Glycocalyx: A Possible Explanation for Molecular Filtering? *Journal of Structural Biology* **2001,** 136, (3), 239-255.

11. Smith, M. L.; Long, D. S.; Damiano, E. R.; Ley, K., Near-wall mu-PIV reveals a hydrodynamically relevant endothelial surface layer in venules in vivo. *Biophys J.* **2003** 85, (1), 637-645.

12. Damiano, E. R.; Long, D. S.; Smith, M. L., Estimation of viscosity profiles using velocimetry data from parallel flows of linearly viscous fluids: application to microvascular haemodynamics. *Fluid Mechanics* **2004** 512, 1-19.

13. Israelachvili, J., Thin film studies using multiple beam interferometry. *J. Colloid Interface Science* **1973,** 44, 259.

14. Israelachvili, J. N., and Adams, G. E., Measurement of Forces between Two Mica Surfaces in Aqueous Electrolyte Solutions in the Range 0-100 nm. *Chem. Soc., Faraday Trans.* **1978,** 74, 975-1001.

15. Lipski, A. M.; Pino, C. J.; Haselton, F. R.; Chen, I.; Shastri, V. P., The effect of silica nanoparticle-modified surfaces on cell morphology, cytoskeletal organization and function. *Biomaterials* **2008,** 29, 3836–3846.

16. Boudreau, N.; Bissell, M. J., Extracellular matrix signaling: integration of form and function in normal and malignant cells. *Curr Opin Cell Biol* **1998,** 10, (5), 640–6.

17. Schwartz, M. A.; Ginsberg, M. H., Networks and crosstalk: integrin signalling spreads. *Nat Cell Biol* **2002,** 4, (4), E65–8.

18. Schor, A. M. S., S.L.; Allen, T.D., Effects of culture conditions on the proliferation, morphology and migration of bovine aortic endothelial cells. *Cell Science* **1983,** 62, 267-85.

19. Banquy, X. R., J-M.; Hildgen, P.; Giasson, S., Direct Measurements of Mechanical and Adhesive Properties of Living Cells Using Surface Force Apparatus. *Aust. J. Chem* **2007,** 60, 638-645.

20. Israelachvili, J., *Intermolecular and Surface Forces*. Second ed.; Harcourt Brace & Company, Publishers: San Diego, CA 92101, 1992.

21. Wanga, J. H.; Goldschmidt-Clermontb, P.; Willea, J.; Yina, F. C.-P., Specificity of endothelialcell reorientation in response to cyclic mechanical stretching. *Journal of Biomechanics* **2001,** 34, 1563–1572.

22. Lulevich, V. e. a., Cell Mechanics Using Atomic Force Microscopy-Based Single Cell Compression. *Langmuir* **2006,** 22, 8151-8155.

23. Tatara, Y., Large Deformation of a Rubber Sphere under under Diametral Compression. Part 1: Theoretical Analysis of Press Apporach Contact Radius and Lateral Extension. *JSME International Journal* **1993,** 36, (2), 190-196.

24. Lulevich, V.; Zink, T.; Chen, H. Y.; Liu, F. T.; Liu, G. Y., Cell Mechanics Using Atomic Force Microscopy-Based Single-Cell Compression. *Langmuir* **2006,** 22, 8151-8155.

25. Landau, L. D.; Lifshitz, E. M., *Theory of Elasticity Vol.7 of Course of Theoretical Physics*. 3 ed.; Butterworth-Heinemann: Oxford, 1995; Vol. 7.

Special Acknowledgments

My infinite thanks to Professor Tonya Kuhl for opening your lab, for guiding me, and providing everything needed for the completion of my degree. You are a wonderful role model and an admirable woman.

Thank you to my committee members, Prof. Longo and Prof. Faller, for providing feedback when it was needed.

Thanks to all my lab mates who shared similar frustrations and enjoyed similar achievements, especially Wei-Po Liao who was my desk neighbor and an ever-present friend.

Especial thanks to all my sources of funding, including the NSF Bridge to the Doctorate and NIH Biotechnology Fellowships.

Thanks to my incredible parents: Maria Guadalupe Alcaraz and Hector Vicente Orozco. I am extremely lucky to be your daughter. I couldn't have asked for better parents. There are just not enough words to express how thankful I am for everything you have done for me.

To my siblings, you are and will always be my motivation to move forward. Thank you for being by my side whenever I need you.

Last but not least, thank you Angel Orduno, my beloved husband, for being with me unconditionally and for being my source of happiness. I love you and cherish you with everything that I am.